



This is a repository copy of *The Modified Manson-Coffin Curve Method to estimate fatigue lifetime under complex constant and variable amplitude multiaxial fatigue loading*.

White Rose Research Online URL for this paper:  
<http://eprints.whiterose.ac.uk/96263/>

Version: Published Version

---

**Article:**

Wang, Y. and Susmel, L. (2016) The Modified Manson-Coffin Curve Method to estimate fatigue lifetime under complex constant and variable amplitude multiaxial fatigue loading. *International Journal of Fatigue*, 83 (2). pp. 135-149. ISSN 0142-1123

<https://doi.org/10.1016/j.ijfatigue.2015.10.005>

---

Article available under the terms of the CC-BY-NC-ND licence  
(<https://creativecommons.org/licenses/by-nc-nd/4.0/>)

**Reuse**

Unless indicated otherwise, fulltext items are protected by copyright with all rights reserved. The copyright exception in section 29 of the Copyright, Designs and Patents Act 1988 allows the making of a single copy solely for the purpose of non-commercial research or private study within the limits of fair dealing. The publisher or other rights-holder may allow further reproduction and re-use of this version - refer to the White Rose Research Online record for this item. Where records identify the publisher as the copyright holder, users can verify any specific terms of use on the publisher's website.

**Takedown**

If you consider content in White Rose Research Online to be in breach of UK law, please notify us by emailing [eprints@whiterose.ac.uk](mailto:eprints@whiterose.ac.uk) including the URL of the record and the reason for the withdrawal request.



[eprints@whiterose.ac.uk](mailto:eprints@whiterose.ac.uk)  
<https://eprints.whiterose.ac.uk/>

## **The Modified Manson-Coffin Curve Method to estimate fatigue lifetime under complex constant and variable amplitude multiaxial fatigue loading**

Yingyu Wang<sup>1, 2</sup> and Luca Susmel<sup>2</sup>

<sup>1</sup>Key Laboratory of Fundamental Science for National Defense-Advanced Design Technology of Flight Vehicle, Nanjing University of Aeronautics and Astronautics, Nanjing, 210016, China

<sup>2</sup>Department of Civil and Structural Engineering, the University of Sheffield, Sheffield S1 3JD, UK

Corresponding Author: Prof. Luca Susmel  
Department of Civil and Structural Engineering  
The University of Sheffield, Mappin Street, Sheffield, S1 3JD, UK  
Telephone: +44 (0) 114 222 5073  
Fax: +44 (0) 114 222 5700  
e-mail: [l.susmel@sheffield.ac.uk](mailto:l.susmel@sheffield.ac.uk)

### **ABSTRACT**

This paper investigates the accuracy of the so-called Modified Manson-Coffin Curve Method (MMCCM) in estimating fatigue lifetime of metallic materials subjected to complex constant and variable amplitude multiaxial load histories. The MMCCM postulates that fatigue damage is maximised on that material plane experiencing the maximum shear strain amplitude. In the present investigation, the orientation of the critical plane was determined through that direction along which the variance of the resolved shear strain reaches its maximum value. Under variable amplitude complex load histories, this direction was also used to count the resolved shear strain cycles via the classic Rain-Flow method. Further, the degree of multiaxiality and non-proportionality of the time-variable stress states at the assumed critical locations was directly quantified through a suitable stress ratio which accounts for (i) the mean value and the variance of the stress perpendicular to the critical plane as well as for (ii) the variance of the shear stress resolved along the direction experiencing the maximum variance of the resolved shear strain. The accuracy and reliability of the proposed approach was checked against approximately 650 experimental data taken from the literature and generated by testing un-notched metallic materials under complex constant and variable amplitude multiaxial load histories. The sound agreement between estimates and experimental results which was obtained strongly supports the idea that the proposed design technique is a powerful engineering tool allowing metallic materials to be designed against constant and variable amplitude multiaxial fatigue by always reaching a remarkable level of accuracy. This approach offers a complete solution to the strain based multiaxial fatigue problem.

**Keywords:** Multiaxial fatigue, Variable amplitude loading, Critical plane

## 1. Introduction

In situations of practical interest, engineering components and structures are subjected to complex time-variable load histories, the applied time-dependent systems of forces/moments resulting in local variable amplitude (VA) multiaxial stress/strain states. Estimating fatigue strength of metallic materials subjected to VA multiaxial load histories is a complex design problem which must be addressed properly in order to avoid unwanted breakages during in-service operations. Owing to the high costs associated with fatigue failures, since the beginning of the last century a tremendous effort has been made by the international scientific community to devise appropriate engineering tools suitable for estimating fatigue damage under complex loading paths. If attention is focused on the low/medium-cycle fatigue regime, examination of the state of the art [1-7] suggests that, so far, this intractable design problem has been addressed mainly by trying to extend the use of well-known constant amplitude (CA) multiaxial fatigue criteria to those situations involving multiaxial VA load histories. In this context, among the methods which have been employed so far, certainly the SWT parameter [8, 9], Brown & Miller's criterion [10, 11], and Fatemi & Socie's critical plane approach [12, 13] deserve to be mentioned explicitly.

As far as VA multiaxial load histories are concerned, accurately performing the cycle counting certainly represents one of the trickiest aspects, the scientific community being still debating to agree a commonly accepted strategy. As to the cycle counting issue, examination of the state of the art suggests that the most successful methodologies [11, 13-15] which have been formalised and validated so far are all based on the use of the classic Rain-Flow Method (this method being originally developed to address simple uniaxial situations [16]).

When it comes to designing components and structures against VA multiaxial fatigue, another tricky problem that must be addressed properly is the definition of an appropriate rule suitable for estimating cumulative damage. Even though a variety of methods have been proposed so far [17], certainly, in situations of practical interest, the most used rule is still the linear one devised by Palmgren [18] and Miner [19]. According to this classic approach, fatigue failure takes place as soon as the damage sum becomes equal to unity. However, accurate experimental investigations have proven that the critical value of the damage sum,  $D_{cr}$ , vary in the range 0.02-5, its average value being equal to 0.27 for steel and to 0.37 for aluminium [20]. Further, given the material,  $D_{cr}$  is seen to vary as the geometry of the component, the degree of multiaxiality of the assessed VA load history, and the profile of the considered load spectrum change [20-22]. Thus, systematically taking the critical value of the damage sum equal to unity may lead, under particularly unfavourable circumstances, to non-conservative estimates. This suggests that  $D_{cr}$  can be evaluated accurately for the specific material/component/load history being assessed solely via expensive and time-consuming experimental trials.

In this complex scenario, this paper reports on an attempt of extending the use of a multiaxial fatigue criterion we have recently proposed [23-25] - here called the Modified Manson-Coffin

Curve Method (MMCCM) - to those situations involving complex CA and VA loading paths. In more detail, such a strain based critical plane approach is attempted here to be applied along with the Maximum Variance concept [26-28] in order to formalise a robust fatigue assessment technique suitable for estimating fatigue lifetime of metallic materials subjected to complex CA and VA multiaxial load histories.

## 2. Fundamentals of the MMCCM

As far as CA loading paths are concerned, the MMCCM [23-25] postulates that fatigue damage in the low/medium-cycle fatigue regime can accurately be estimated via the stress and strain components acting on that material plane (i.e., the so-called critical plane) experiencing the maximum shear strain amplitude,  $\gamma_a$ . The degree of multiaxiality and non-proportionality of the applied load history as well as the presence of non-zero mean stresses are quantified by the MMCCM via the shear stress amplitude,  $\tau_a$ , relative to the plane of maximum shear strain amplitude and the amplitude,  $\sigma_{n,a}$ , and the mean value,  $\sigma_{n,m}$ , of the stress normal to the critical plane. The definitions which are proposed here as being adopted to calculate the stress/strain quantities of interest not only under CA, but also under VA multiaxial fatigue loading will be discussed in the next section in great detail.

The fatigue damage model on which the MMCCM is based is shown in Figure 1a. According to this schematisation, Stage I cracks are assumed to initiate on those crystallographic planes most closely aligned with the maximum shear strain direction [29]. The subsequent propagation phenomenon is strongly influenced by the stress perpendicular to the critical plane [9, 30]. In particular, the amplitude of the stress normal to the critical plane,  $\sigma_{n,a}$ , favours the growth process by cyclically opening and closing the micro/meso fatigue cracks [31]. The propagation phase is also influenced by the mean stress,  $\sigma_{n,m}$ , normal to the plane of maximum shear strain amplitude. In fact, a tensile superimposed static normal stress tends to keep the micro/meso fatigue cracks open by minimising the interactions amongst the crack surfaces' asperities [9, 30]. This favours the effect of the cyclic shear stress which pushes the tips of the cracks themselves [32]. On the contrary, under compressive mean normal stresses, the resulting additional frictional phenomena between the crack surfaces [9, 30] mitigate the action of the cyclic shear stress [32], this resulting in a reduction of the crack growth rate.

According to the fatigue damage model depicted in Figure 1a, the degree of multiaxiality and non-proportionality of the stress state damaging the assumed crack initiation locations is quantified by the MMCCM via the following critical plane stress ratio [23]:

$$\rho = \frac{\sigma_{n,m} + \sigma_{n,a}}{\tau_a} = \frac{\sigma_{n,max}}{\tau_a} \quad (1)$$

In definition (1)  $\tau_a$  is the shear stress amplitude relative to the critical plane, whilst  $\sigma_{n,m}$ ,  $\sigma_{n,a}$  and  $\sigma_{n,max}$  are the mean value, the amplitude and the maximum value of the stress perpendicular to the plane of maximum shear strain amplitude, respectively. Ratio  $\rho$  is seen to be capable of modelling not only the presence of superimposed static stresses, but also the degree of multiaxiality and non-proportionality of the applied load history [23, 31]. In particular, as suggested by Socie [9, 30], the effect of the stress components perpendicular to the critical plane can efficiently be modelled by simply using the maximum normal stress, since  $\sigma_{n,max} = \sigma_{n,m} + \sigma_{n,a}$ . This simple strategy was followed by Socie himself to reformulate the SWT parameter to make it suitable for performing the multiaxial fatigue assessment of those metals whose mesoscopic cracking behaviour is mainly Mode I governed [9]. Similarly, the normal maximum stress,  $\sigma_{n,max}$ , was employed by Fatemi and Socie to devise their shear strain based critical plane approach [12]. The well-known accuracy and reliability of these two criteria should fully support the idea that  $\sigma_{n,max}$  is a stress quantity capable of accurately taking into account the mean stress effect in multiaxial fatigue. This holds true provided that  $\sigma_{n,max}$  is consistently used with an appropriate fatigue damage model, the damage model on which the MMCCM is based being shown in Figure 1a.

Turning back to definition (1), it is evident that under VA fatigue loading the value of ratio  $\rho$  may vary cycle by cycle. Accordingly, appropriate definitions for the stress quantities of interest are required in order to consistently calculate the  $\rho$  ratio also in the presence of complex VA multiaxial load history. The strategy we propose to address the VA problem will be discussed in Section 3 in detail.

Under fatigue loading, there are always at least two planes experiencing the maximum shear strain amplitude, this holding true independently from the complexity of the assessed load history. Therefore, amongst all the potential critical planes, the one which must be considered to estimate fatigue lifetime is the one characterised by the largest value of ratio  $\rho$  [31].

To quantify the fatigue damage extent, the MMCCM makes use of non-conventional Manson-Coffin curves, where the values of the required calibration constants vary as the critical plane stress ratio,  $\rho$ , changes [5]. The way this method works can be depicted in a log-log diagram where the shear strain amplitude,  $\gamma_a$ , relative to the critical plane is plotted against the number of reversals to failure,  $2N_f$  (Fig. 1b). As shown in Figure 1b, different modified Manson-Coffin curves are obtained as ratio  $\rho$  varies, each of these curves being described mathematically as follows:

$$\gamma_a = \frac{\tau'_f(\rho)}{G} (2N_f)^{b(\rho) + \gamma'_f(\rho)} \cdot (2N_f)^{c(\rho)} \quad (2)$$

Given the material, constants  $\tau'_f(\rho)$ ,  $\gamma'_f(\rho)$ ,  $b(\rho)$  and  $c(\rho)$  can directly be derived from the fully-reversed uniaxial and torsional Manson-Coffin fatigue curves re-written according to Tresca's hypotheses, i.e. [31]:

$$\gamma_a = (1 + \nu_e) \frac{\sigma'_f}{E} (2N_f)^b + (1 + \nu_p) \epsilon'_f (2N_f)^c \quad (\text{Uniaxial case, } \rho=1) \quad (3)$$

$$\gamma_a = \frac{\tau'_f}{G} (2N_f)^{b_0} + \gamma'_f (2N_f)^{c_0} \quad (\text{Torsional case, } \rho=0) \quad (4)$$

where  $\nu_e$  and  $\nu_p$  are Poisson's ratio for elastic and plastic strain, respectively. By manipulating Eqs (3) and (4) under some simplifying hypotheses [23], the material constants in Eq. (1) can be expressed explicitly as follows [23, 31]:

$$\frac{\tau'_f(\rho)}{G} = \rho \cdot (1 + \nu_e) \frac{\sigma'_f}{E} + (1 - \rho) \frac{\tau'_f}{G} \quad (5)$$

$$\gamma'_f(\rho) = \rho \cdot (1 + \nu_p) \epsilon'_f + (1 - \rho) \gamma'_f \quad (6)$$

$$b(\rho) = \frac{b \cdot b_0}{(b_0 - b)\rho + b} \quad (7)$$

$$c(\rho) = \frac{c \cdot c_0}{(c_0 - c)\rho + c} \quad (8)$$

To conclude, it is worth observing that, according to the above definitions, the modified Manson-Coffin curves move upwards as ratio  $\rho$  decreases (see Figure 1b). In other words, the MMCCM estimates fatigue lifetime by assuming that, for a given value of the shear strain amplitude acting on the critical plane, the fatigue damage extent increases with increasing of ratio  $\rho$ : this explains why when selecting the critical plane amongst those experiencing the maximum shear strain amplitude, the one to be used is that characterised by the largest value of ratio  $\rho$ .

### 3. The Maximum Variance concept to determine the stress/strain quantities relative to the critical plane

In order to apply the MMCCM to estimate fatigue lifetime of metallic materials subjected to uniaxial/multiaxial fatigue loading, the first problem to be addressed is the determination of those stress/strain quantities relative to the critical plane which are required to quantify the fatigue damage extent. As discussed in what follows, in the present investigation such quantities are suggested as being estimated by taking full advantage of the maximum variance concept [26].

From a statistical point of view, the variance of a time-variable signal is equal to the expected value of the squared deviation from the mean. In other words, by definition, the variance quantifies the amount of variation (within the two extremes delimiting the maximum range) associated, over the time interval,  $T$ , of interest, with the signal being investigated. According to this definition, the variance is a statistical quantity which is independent from the mean value of the considered signal. If attention is focussed specifically on time-variable load histories, the variance of a stress/strain signal is seen to be related to the amount of damage caused by the signal itself [33, 34]. The variance approach assumes that the damage in the candidate plane can be estimated from a root mean square calculation. It is well-known that the dependence between shear amplitudes and damage may involve exponents having value different from two. Accordingly, under very specific circumstances, more accurate estimates may be obtained by adopting higher central moments of the resolved shear strain history, instead of the second central moment. However, much experimental evidence (please, see Refs [26, 33, 34] and references reported therein) suggests that, in situation of practical interest, the use of the variance concept allows VA load histories to be post-processed by always reaching an adequate level of accuracy. Recently, this idea [27, 28] has successfully been applied along with the stress based critical plane concept to estimate fatigue lifetime under uniaxial/multiaxial VA multiaxial fatigue loading [35-40]. In light of the high level of accuracy obtained in the long-life fatigue regime, the next logical step is then reformulating the maximum variance idea to make it suitable for being applied in terms of cyclic strains. The fundamental concepts on which the Shear Strain Maximum Variance Method ( $\gamma$ -MVM) is based are summarised in what follows, whereas its mathematical formalisation is discussed in detail in Appendix A.

The  $\gamma$ -MVM takes as a starting point the assumption that the critical plane is that material plane containing the direction, MV, that experiences the maximum variance of the resolved shear strain,  $\gamma_{MV}(t)$  – see Figures 2a and 2b. If this direction as well as the orientation of the associated material plane are known, direction MV together with the unit vector normal to the critical plane can directly be used to calculate the stress/strain quantities of interest. In more detail, under CA fatigue loading, the amplitudes and the mean values of the shear strain and shear stress component relative to the critical plane can directly be calculated as follows (see also Figure 2c):

$$\gamma_a = \frac{1}{2} \left( \gamma_{MV, \max} - \gamma_{MV, \min} \right) \quad (9)$$

$$\gamma_m = \frac{1}{2} \left( \gamma_{MV, \max} + \gamma_{MV, \min} \right) \quad (10)$$

Please, cite this paper as: Wang, Y., Susmel, L. The Modified Manson-Coffin Curve Method to estimate fatigue lifetime under complex constant and variable amplitude multiaxial fatigue loading. International Journal of Fatigue 83 (2), pp. 135-149, 2016.

---

$$a = \frac{2}{\tau_{MV, \min}}$$

$$\tau_m = \frac{1}{2} \left( \tau_{MV,max} + \tau_{MV,min} \right) \quad (12)$$

In definitions (9) and (10)  $\gamma_{MV,max}$  and  $\gamma_{MV,min}$  are the maximum and minimum value of  $\gamma_{MV}(t)$ , respectively. Similarly, in definitions (11) and (12)  $\tau_{MV,max}$  and  $\tau_{MV,min}$  denote the maximum and minimum value of the shear stress,  $\tau_{MV}(t)$ , resolved along direction MV, respectively (Fig. 2c).

By following the same strategy as above, under CA fatigue loading the amplitude,  $\sigma_{n,a}$ , and the mean value,  $\sigma_{n,m}$ , of the stress normal to the critical plane,  $\sigma_n(t)$ , can be calculated as follows:

$$\sigma_{n,a} = \frac{1}{2} \left( \sigma_{n,max} - \sigma_{n,min} \right) \quad (13)$$

$$\sigma_{n,m} = \frac{1}{2} \left( \sigma_{n,max} + \sigma_{n,min} \right), \quad (14)$$

where  $\sigma_{n,max}$  and  $\sigma_{n,min}$  are used to denote the maximum and minimum value of normal stress  $\sigma_n(t)$ , respectively (Fig. 2c).

Turning to VA situations, assume now that the critical point O in the component being assessed (Fig. 2a) is damaged by a stress/strain state whose components vary randomly in the time interval of interest, i.e., time interval [0, T]. As soon as the orientation of the direction, MV, experiencing the maximum variance of the resolved shear strain is known (Fig. 2b), the mean value and the variance of the shear strain and shear stress component relative to the critical plane can directly be determined as follows (see also Figure 2d):

$$\gamma_m = \frac{1}{T} \int_0^T \gamma_{MV}(t) \cdot dt \quad (15)$$

$$\text{Var}[\gamma_{MV}(t)] = \frac{1}{T} \int_0^T [\gamma_{MV}(t) - \gamma_m]^2 \cdot dt \quad (16)$$

$$\tau_m = \frac{1}{T} \int_0^T \tau_{MV}(t) \cdot dt \quad (17)$$

$$\text{Var}[\tau_{MV}(t)] = \frac{1}{T} \int_0^T [\tau_{MV}(t) - \tau_m]^2 \cdot dt \quad (18)$$

Please, cite this paper as: Wang, Y., Susmel, L. The Modified Manson-Coffin Curve Method to estimate fatigue lifetime under complex, constant and variable amplitude, multi-axial fatigue loading. *International Journal of Fatigue* 83 (2), pp. 135-149, 2016.

The variance terms determined as above allow the equivalent amplitude of the shear stress and shear strain resolved along direction MV to be determined according to the following trivial relationships:

$$\gamma_a = \sqrt{2 \cdot \text{Var}[\gamma_{MV}(t)]} \quad (19)$$

$$\tau_a = \sqrt{2 \cdot \text{Var}[\tau_{MV}(t)]} \quad (20)$$

In a similar way, the equivalent amplitude and the mean value of the stress perpendicular to the critical plane,  $\sigma_n(t)$ , can be determined as follows:

$$\sigma_{n,a} = \sqrt{2 \cdot \text{Var}[\sigma_n(t)]} \quad (21)$$

$$\sigma_{n,m} = \frac{1}{T} \int_0^T \sigma_n(t) \cdot dt \quad (22)$$

where:

$$\text{Var}[\sigma_n(t)] = \frac{1}{T} \int_0^T [\sigma_n(t) - \sigma_{n,m}]^2 \cdot dt \quad (23)$$

To conclude, it is worth observing that the  $\gamma$ -MVM has two key advantages over the other existing methods. First, it is very efficient from a computational point of view. In fact, as soon as the variance and covariance terms of the components of the strain tensor being post-processed are known, the time required to determine the orientation of the critical plane is almost independent from the length of the assessed load history. Second, since  $\gamma_{MV}(t)$  and  $\tau_{MV}(t)$  are monodimensional quantities, the cycle counting under multiaxial fatigue loading can be performed rigorously by using one of those techniques specifically devised by considering uniaxial fatigue situations (and, in particular, via the Rain-Flow counting method [16]).

#### 4. The MMCCM to estimate fatigue lifetime under CA and VA multiaxial fatigue loading

The last step in the formalisation of the proposed design technique is the definition of standard procedures suitable for using this approach in situations of practical interest to estimate lifetime of metallic materials subjected to in-service CA and VA load histories.

Consider then the component sketched in Figure 3a which is assumed to be subjected to a CA load history. As soon as the direction experiencing the maximum variance of the resolved shear strain is known (Fig. 3b), the amplitude of the shear strain relative to the critical plane,  $\gamma_a$ , can easily be determined according to definition (9) – see Figure 3c. Similarly, the shear stress amplitude,  $\tau_a$ , and the maximum normal stress,  $\sigma_{n,max}$ , relative to the critical plane (Figs 3d and 3e) can directly be calculated through Eqs (11), (13) and (14). These stress quantities allow the critical plane stress

ratio, Eq. (1), characterising the load history being assessed to be determined unambiguously (Fig. 3f). Through the calculated value for  $\rho$ , the constants in the MMCCM can now be estimated (Fig. 3g) from the fully-reversed uniaxial and torsional fatigue properties via relationships (5) to (8). These constants can then be used to derive, for the calculated value of  $\rho$ , the required Modified Manson-Coffin curve (Fig. 3h). Finally, the shear strain amplitude relative to the critical plane,  $\gamma_a$ , together with Eq. (2) allows the number of cycles to failure to be estimated directly (Fig. 3h).

Turning to VA multiaxial fatigue situations, the first problem which has to be addressed is the formalisation of a strategy allowing the cycle counting to be performed so that the fatigue damage extent can be quantified accurately. As briefly discussed in Section 2, the MMCCM assumes that the critical plane is the one containing the direction experiencing the maximum variance of the resolved shear strain (Fig. 1a). According to Kanazawa, Miller and Brown [29], Stage I cracks form on those slip planes most closely aligned to the macroscopic planes of maximum shear. Accordingly, the hypothesis can be formed that, under VA fatigue loading, the resolved shear strain,  $\gamma_{MV}(t)$ , is the strain quantity to be used to perform the cycle counting. Therefore, owing to the fact that  $\gamma_{MV}(t)$  is a monodimensional strain quantity, given a load history, the corresponding cumulative shear strain spectrum can directly be determined by using the Rain-Flow method [16].

Having formed this initial hypothesis, consider now the component of Figure 4a which is assumed to be subjected to a complex system of time variable forces and moments which result in a local VA state of stress/strain at critical point O. As soon as the direction of maximum variance is known (Fig. 4b), the equivalent amplitude of the shear stress relative to the critical plane,  $\tau_a$ , can be determined according to definition (20), whereas the equivalent value of the maximum stress perpendicular to the critical plane can directly be estimated via definitions (21) and (22), where  $\sigma_{n,max} = \sigma_{n,m} + \sigma_{n,a}$  (see Figures 4d and 4e). Stress quantities  $\tau_a$  and  $\sigma_{n,max}$  allow then the critical plane stress ratio,  $\rho$ , to be determined under VA fatigue loading via definition (1) – see Figure 4f. This ratio can now be used to estimate the constants in the MMCCM according to definitions (5) to (8) – see Figures 4g and 4h. In parallel, by taking full advantage of the Rain-Flow Method (Fig. 4i), signal  $\gamma_{MV}(t)$  has to be post-processed in order to build the corresponding shear strain spectrum (Fig. 4j). This spectrum along with the estimated modified Manson-Coffin curve, Eq. (2), allow the damage content associated with any counted shear strain cycles to be quantified (see Figures 4h and 4k). Finally, the number of cycles to failure can directly be estimated as follows:

$$D_{tot} = \sum_{i=1}^j \frac{n_i}{N_{f,i}} \Rightarrow N_{f,e} = \frac{D_{cr}}{\sum_{i=1}^j \frac{n_i}{N_{f,i}}} \quad (24)$$

where  $D_{tot}$  is the total value of the damage sum.  $D_{cr}$  is instead the critical value of the damage sum, i.e., the value of  $D_{tot}$  resulting in the initiation of a fatigue crack in the metallic material being

assessed. It is worth observing here that according to the classic theory due to Palmgren [18] and Miner [19],  $D_{cr}$  should be invariably equal to unity. On the contrary, as observed by Sonsino [5], in situations of practical interest its value is seen to range in the interval 0.02-5.

Under VA multiaxial fatigue loading, ratio  $\rho$  is determined by post-processing the entire local load history projected along the direction of maximum variance of the resolved shear strain as well as along the direction perpendicular to the critical plane. The value for ratio  $\rho$  calculated according to this strategy is then used to estimate the specific modified Manson-Coffin curve that has to be used to quantify the damage content associated with the counted cycles. This means that, given the material, different VA multiaxial load histories are assessed by using the same modified Manson-Coffin curve as long as they are characterised by the same value of ratio  $\rho$ . However, even if  $\rho$  is the same, in the most general case, different VA load histories are expected to result in different values of the estimated number of cycles to failure, this depending on the specific profile of the corresponding shear strain spectrum (Fig. 4j). Another important aspect is that the shear strain spectrum is built by post processing the actual strain history resolved along the direction experiencing the maximum variance of the resolved shear strain. This allows the sequence effect to be taken into account effectively. The above ideas represent the key concepts on which the proposed approach is based, the validity of this *modus operandi* being checked in the next section by post-processing a large number of experimental results taken from the literature.

To conclude, it is worth emphasising the fact that both under CA and VA fatigue loading the MMCCM must be applied by post-processing the actual elasto-plastic time-variable stresses and strains damaging the assumed critical location. This implies that appropriate techniques must be employed in order to perform the stress/strain analysis by accurately quantifying/modelling important phenomena such as strain hardening/softening, non-proportional hardening, ratcheting, memory effect, mean stress relaxation, etc.

## 5. Validation by experimental data

In order to check the accuracy and reliability of the proposed design methodology, about 650 experimental results were selected from the technical literature. Table 1 summarises the static and fatigue properties of the investigated metallic materials. For the majority of the considered data sets, the required material properties were directly available in the original sources. In some cases, even though the required fatigue constants were not listed explicitly,  $K'$ ,  $n'$ ,  $\sigma'_f$ ,  $\epsilon'_f$ ,  $b$ ,  $c$ ,  $\tau'_f$ ,  $\gamma'_f$ ,  $b_o$ , and  $c_o$  were directly calculated by post-processing the fully-reversed uniaxial and torsional experimental results being provided. In particular, given the population of data, the required parameters were determined, for a probability of survival equal to 50%, via a linear regression model (in a log-log representation) optimised by using the least-squares method [58]. The material parameters quantified according to this procedure are clearly indicated in Table 1. When solely the constants of the fully-reversed torsional Manson-Coffin curves were not available, they were

estimated from the corresponding uniaxial fatigue constants by using von Mises' criterion [7, 31], i.e.:

$$\tau'_f = \frac{\sigma'_f}{\sqrt{3}}; \gamma'_f = \sqrt{3}\varepsilon'_f; b_0 = b; c_0 = c \quad (25)$$

All the considered data were generated by controlling the local deformations during testing, so that in the majority of the sources the corresponding stress histories were not given. In order to calculate the stress components relative to the critical plane when the relevant time-variable stress histories were not directly available, the required elasto-plastic stress states were estimated by using Jiang and Sehitoglu's method [59, 60]. Finally, in those cases in which the values of the non-proportional cyclic strength coefficient,  $K'_{NP}$ , and the non-proportional cyclic strain hardening exponent,  $n'_{NP}$ , were not determined experimentally, non-proportional hardening was modelled by taking the constants in the corresponding Ramberg-Osgood type equation as follows [7]:

$$K'_{NP} = 1.25 \cdot K_{NP}; n'_{NP} = n' \quad (26)$$

Since a number of assumptions were made to make the selected experimental data suitable for performing a systematic validation exercise, the first problem to address was the definition of a reference error band allowing the accuracy of the proposed fatigue design approach to be assessed quantitatively. The estimated,  $N_{f,e}$ , vs. experimental,  $N_f$ , number of cycles to failure diagram reported in Figure 6a shows the accuracy of the conventional approach due to Manson and Coffin in estimating the fatigue lifetime of the considered materials under pure axial and pure torsional fully-reversed loading, the corresponding loading paths being sketched in Figure 5. This chart shows that the experimental points fall within an error band of 3. Accordingly, such an error band will be used in what follows to quantify the accuracy of the proposed approach. This choice can be justified by observing that, from a statistical viewpoint, the systematic usage of a predictive method cannot obviously result in an accuracy level which is higher than the intrinsic scatter characterising the information used to calibrate the method itself. Another important aspect which deserves to be recalled here is that under non-proportional/complex loading paths the principal directions rotate during the loading cycle. This results in the simultaneous activation of several slip systems so that Stage I cracks tend to initiate on several material planes by subsequently propagating along certain paths whose orientation depends not only on the characteristics of the applied stress/strain history, but also on the local material morphology [29]. On the contrary, under proportional loading micro-cracks are seen to initiate on preferential material planes, resulting in smaller deviations of the propagation directions with respect to the one of maximum shear strain [29]. According to the

above considerations, complex/non-proportional load histories are expected to be characterised by a larger degree of scattering compared with the corresponding proportional/simple cases.

In order to check the accuracy of the MMCCM applied along with the  $\gamma$ -MVM, initially our fatigue assessment methodology was used to estimate fatigue lifetime under CA fatigue loading, the considered loading paths being shown in Figure 5. The error diagram reported in Figure 6b makes it evident that our approach was highly accurate, its systematic usage resulting in predictions failing mainly within the target error interval. It is worth observing that such a high level of accuracy was reached not only in the presence of proportional and non-proportional sinusoidal/triangular strain paths, but also under complex CA load histories. Further, the MMCCM used in conjunction with the  $\gamma$ -MVM was seen to be capable of accurately taking into account the effect of superimposed static strains as well (see Figure 6b).

Subsequently, our fatigue assessment method was used to predict the fatigue lifetime of samples of Al7075-T651 [41], S460N [48] and 304SS [55] tested under combined CA axial and torsional sinusoidal/triangular strain signals of different frequencies. By focussing attention on the considered sinusoidal load histories, it is possible to observe that under a ratio between the frequency of the axial channel,  $F_x$ , and the frequency of the torsional channel,  $F_{xy}$ , equal to 2, the resulting stress/strain history relative to the critical plane was composed of one shear stress/strain cycle and two normal stress cycles (see Path F in Figure 7). On the contrary, the use of the proposed method resulted in two shear stress/strain cycles under a  $F_x$  to  $F_{xy}$  ratio equal to 0.5 (Path G in Figure 7) and in four shear stress/strain cycles under  $F_x/F_{xy}=0.25$  (Path H in Figure 7). In other words, for these two loading paths one nominal cycle was composed of two and four shear cycles under a  $F_x$  to  $F_{xy}$  ratio equal to 0.5 and 0.25, respectively. Since a similar reasoning applies also to the triangular strain paths sketched in Figure 7 (see Paths I to M), this explains the reason why the error diagram in Figure 7 was plotted in terms of number of blocks to failure, one block corresponding to one nominal cycle. The  $N_{f,e}$  vs.  $N_f$  chart of Figure 7 shows that the proposed approach was highly accurate in modelling the damaging effect of combined CA axial and torsional strain signals of different frequencies. As to the obtained level of accuracy, it is important to point out that it was reached by taking the critical value of the damage sum,  $D_{cr}$ , equal to unity for Al7075-T651 [41] and S460N [48], whereas, as suggested by Sonsino [20], it was set equal to 0.27 for 304SS [55].

Subsequently, attention was focussed on the accuracy of the proposed design approach in modelling the sequence effect. In particular, our method was attempted to be used to estimate the fatigue lifetime of specimens of 304SS [54], pure titanium [14], titanium BT9 [14], SNCM439 [55], SNCM630 (A) [56] and SNCM630 (B) [55] tested under different combinations of axial (A), torsion (T), in-phase (I) and 90° out-of-phase (O) axial/torsion cycles. Such load histories were built as a sequence of fully-reversed CA loading blocks containing a predefined number of cycles. Sequences AA and TT were formed of two axial and two torsional blocks characterised by different

amplitudes. The error diagram reported in Figure 8 confirms that the MMCCM applied along with the  $\gamma$ -MVM was capable of accurately predicting the sequence effect in fatigue, the critical value of the damage sum,  $D_{cr}$ , being taken equal to unity for all the investigated materials.

The next step in the performed validation exercise was considering short VA load histories. The obtained results are summarised in the error diagram of Figure 9, whereas the profile of the considered nominal loading paths are sketched in Figure 5. In order to show how our design technique works in the presence of short VA loading blocks, the load histories re-calculated in terms of stress/strain quantities relative to the critical plane are reported in Figure 9 for Paths RO1, RO2 and RO3. This figure makes it evident that, although Path RO1 and RO2 may appear very similar, in the case of Path RO1 the use of our approach resulted in four shear cycles, whereas for Path RO2 a nominal loading block contained one shear stress/strain cycle. The estimated vs. experimental number of blocks to failure diagram of Figure 9 confirms that the MWCM applied along with the  $\gamma$ -MVM was highly accurate also in estimating lifetime under short VA load histories, with predictions falling within the target error band.

Subsequently, we focussed our attention on the results generated by Shamsaei, Fatemi and Socie [15] by testing thin-walled tubular specimens of 1050 QT and 304L stainless steel under the discriminating strain paths shown both in Figure 5 and in Figure 10. In more detail, Paths FR contained a series of fully-reversed in-phase axial/torsion cycles applied by making angle  $\xi$  vary (see Figure 10). Both Path FRI and Path FRR were characterised by a step angle  $\Delta\xi$  equal to  $1^\circ$ , with  $\xi$  ranging in the interval  $0^\circ$ - $360^\circ$ . Paths FRI were generated by gradually increasing angle  $\xi$  from  $0^\circ$  to  $360^\circ$ , whereas Paths FRR contained cycles applied in random order. Path FRI15 had  $\Delta\xi=15^\circ$  with  $0^\circ \leq \xi \leq 360^\circ$ , whereas for Path FRI90  $\Delta\xi$  was equal to  $90^\circ$ , with  $\xi$  gradually increasing from  $0^\circ$  to  $270^\circ$ . Paths PI contained pulsating axial/torsion in-phase cycles with  $\Delta\xi=1^\circ$  and  $0^\circ \leq \xi \leq 360^\circ$ . Similarly, Paths PI90 was formed of four ( $\Delta\xi=90^\circ$ ) pulsating in-phase axial/torsion cycles with  $0^\circ \leq \xi \leq 270^\circ$ . Some examples showing the resolved shear strain spectra determined by applying the  $\gamma$ -MVM are reported in Figure 10. The error diagram of Figure 10 confirms that the MMCCM was capable of estimates falling within the target error band. As to the made predictions, it is worth observing that a higher degree of conservatism could have been obtained by simply setting, as suggested by Sonsino [20], the critical value of the damage sum,  $D_{cr}$ , equal to 0.27.

Finally, the accuracy of the MMCCM applied along with the  $\gamma$ -MVM was checked against the results generated by Vormwald and co-workers [49] by testing tubular samples of Al5083 and S460N under the in-phase and  $90^\circ$  out-of-phase strain spectrum reported in Figure 11. This linear spectrum with an omission level of 20% contained 4256 fully-reversed cycles, the ratio between the amplitude of the axial strain,  $\varepsilon_{x,a}$ , and the amplitude of the shear strain,  $\gamma_{xy,a}$ , being constant and equal to 0.577. In the strain spectrum reported in Figure 11  $\sigma_{x,MAX}$ ,  $\tau_{xy,MAX}$  and  $\gamma_{MV,MAX}$  are used to denote, for any tests, the corresponding maximum value in the applied loading blocks. The error

diagram of Figure 11 proves that the use of our multiaxial fatigue lifetime estimation technique resulted in estimates falling within the target error band. It is possible to conclude by observing that, as recommended by Sonsino [20], the above predictions were made by taking  $D_{cr}$  equal to 0.27 for S460N and equal to 0.37 for Al5083.

## 6. Conclusions

- The MMCCM applied along with the  $\gamma$ -MVM is seen to be highly successful in estimating lifetime of metallic materials subjected to CA and VA multiaxial load histories.
- The use of the  $\gamma$ -MVM allows the computational time required to calculate the stress/strain quantities relative to the critical plane to be reduced remarkably: this can help to minimise the costs associated with the design process, this being done by always reaching a remarkable level of accuracy.
- Under VA load histories, if the critical value of the damage sum cannot be determined experimentally, the proposed approach should be applied by taking  $D_{cr}$  equal to (or lower than) 0.27 for steel and 0.37 for aluminium.
- As far as un-notched metallic materials are concerned, the MMCCM applied along with the  $\gamma$ -MVM offers a complete solution to the strain based multiaxial fatigue problem.
- More works need to be done in this area to extend the use of the proposed multiaxial fatigue life estimation technique to metallic components containing notches.

## Appendix A. Mathematical formalisation of the $\gamma$ -MVM

The body of Figure 2a is subjected to a complex system of forces and moments resulting in tri-axial time-variable states of stress and strain damaging internal reference point O. This point is used to define also a suitable local system of coordinates, Oxyz. The following tensors are used to summarise the states of stress and strain at point O (where  $t \in T$ ):

$$[\sigma(t)] = \begin{bmatrix} \sigma_x(t) & \tau_{xy}(t) & \tau_{xz}(t) \\ \tau_{xy}(t) & \sigma_y(t) & \tau_{yz}(t) \\ \tau_{xz}(t) & \tau_{yz}(t) & \sigma_z(t) \end{bmatrix} \quad (A1)$$

$$[\varepsilon(t)] = \begin{bmatrix} \varepsilon_x(t) & \frac{\gamma_{xy}(t)}{2} & \frac{\gamma_{xz}(t)}{2} \\ \frac{\gamma_{xy}(t)}{2} & \varepsilon_y(t) & \frac{\gamma_{yz}(t)}{2} \\ \frac{\gamma_{xz}(t)}{2} & \frac{\gamma_{yz}(t)}{2} & \varepsilon_z(t) \end{bmatrix} \quad (A2)$$

In the above tensors  $\sigma_i(t)$  and  $\varepsilon_i(t)$  ( $i=x, y, z$ ) are the normal stress and normal strain components, whereas  $\tau_{ij}(t)$  and  $\gamma_{ij}(t)$  ( $i, j=x, y, z$ ) are the shear stress and shear strain components.

Angles  $\phi$  and  $\theta$  as shown in Figure A1 can be used to define the orientation of a generic material plane,  $\Delta$ , via its normal unit vector,  $\mathbf{n}$ . According to the above schematisation,  $\phi$  is the angle between the projection of unit vector  $\mathbf{n}$  on the x-y plane and the x-axis, whereas  $\theta$  is the angle between unit vector  $\mathbf{n}$  and the z-axis. A second frame of reference, Oanb, can also be defined as shown in Figure A2, where the unit vectors giving the orientation of the three axes are as follows:

$$\mathbf{n} = \begin{bmatrix} n_x \\ n_y \\ n_z \end{bmatrix} = \begin{bmatrix} \sin(\theta)\cos(\phi) \\ \sin(\theta)\sin(\phi) \\ \cos(\theta) \end{bmatrix}; \mathbf{a} = \begin{bmatrix} a_x \\ a_y \\ a_z \end{bmatrix} = \begin{bmatrix} \sin(\phi) \\ -\cos(\phi) \\ 0 \end{bmatrix}; \mathbf{b} = \begin{bmatrix} b_x \\ b_y \\ b_z \end{bmatrix} = \begin{bmatrix} \cos(\theta)\cos(\phi) \\ \cos(\theta)\sin(\phi) \\ -\sin(\theta) \end{bmatrix} \quad (\text{A3})$$

Given a generic direction on the  $\Delta$  plane which passes through point O (Fig. A1), the associated unit vector,  $\mathbf{q}$ , is as follows:

$$\mathbf{q} = \begin{bmatrix} q_x \\ q_y \\ q_z \end{bmatrix} = \begin{bmatrix} \cos(\alpha)\sin(\phi) + \sin(\alpha)\cos(\theta)\cos(\phi) \\ -\cos(\alpha)\cos(\phi) + \sin(\alpha)\cos(\theta)\sin(\phi) \\ -\sin(\alpha)\sin(\theta) \end{bmatrix} \quad (\text{A4})$$

In definition (A4)  $\alpha$  is the angle between direction  $\mathbf{q}$  and the a-axis (Fig. A1).

The instantaneous values of the stress,  $\sigma_n(t)$ , and strain,  $\varepsilon_n(t)$ , normal to the  $\Delta$  plane can directly be determined as:

$$\sigma_n(t) = \begin{bmatrix} n_x & n_y & n_z \end{bmatrix} \begin{bmatrix} \sigma_x(t) & \tau_{xy}(t) & \tau_{xz}(t) \\ \tau_{xy}(t) & \sigma_y(t) & \tau_{yz}(t) \\ \tau_{xz}(t) & \tau_{yz}(t) & \sigma_z(t) \end{bmatrix} \begin{bmatrix} n_x \\ n_y \\ n_z \end{bmatrix} \quad (\text{A5})$$

$$\varepsilon_n(t) = \begin{bmatrix} n_x & n_y & n_z \end{bmatrix} \begin{bmatrix} \varepsilon_x(t) & \frac{\gamma_{xy}(t)}{2} & \frac{\gamma_{xz}(t)}{2} \\ \frac{\gamma_{xy}(t)}{2} & \varepsilon_y(t) & \frac{\gamma_{yz}(t)}{2} \\ \frac{\gamma_{xz}(t)}{2} & \frac{\gamma_{yz}(t)}{2} & \varepsilon_z(t) \end{bmatrix} \begin{bmatrix} n_x \\ n_y \\ n_z \end{bmatrix} \quad (\text{A6})$$

The shear stress,  $\tau_q(t)$ , and shear strain,  $\gamma_q(t)$ , resolved along direction  $\mathbf{q}$  can instead be determined via the components of unit vector  $\mathbf{q}$ , i.e.:

$$\tau_q(t) = \begin{bmatrix} q_x & q_y & q_z \end{bmatrix} \begin{bmatrix} \sigma_x(t) & \tau_{xy}(t) & \tau_{xz}(t) \\ \tau_{xy}(t) & \sigma_y(t) & \tau_{yz}(t) \\ \tau_{xz}(t) & \tau_{yz}(t) & \sigma_z(t) \end{bmatrix} \begin{bmatrix} n_x \\ n_y \\ n_z \end{bmatrix} \quad (\text{A7})$$

$$\frac{\gamma_q(t)}{2} = \begin{bmatrix} q_x & q_y & q_z \end{bmatrix} \begin{bmatrix} \varepsilon_x(t) & \frac{\gamma_{xy}(t)}{2} & \frac{\gamma_{xz}(t)}{2} \\ \frac{\gamma_{xy}(t)}{2} & \varepsilon_y(t) & \frac{\gamma_{yz}(t)}{2} \\ \frac{\gamma_{xz}(t)}{2} & \frac{\gamma_{yz}(t)}{2} & \varepsilon_z(t) \end{bmatrix} \begin{bmatrix} n_x \\ n_y \\ n_z \end{bmatrix} \quad (\text{A8})$$

Alternatively, shear strain  $\gamma_q(t)$  can also be expressed via the following scalar product:

$$\frac{\gamma_q(t)}{2} = \mathbf{d} \bullet \mathbf{e}(t), \quad (\text{A9})$$

where  $\mathbf{d}$  is the vector of direction cosines:

$$\mathbf{d} = \begin{bmatrix} n_x q_x & n_y q_y & n_z q_z & n_x q_y + n_y q_x & n_x q_z + n_z q_x & n_y q_z + n_z q_y \end{bmatrix}, \quad (\text{A10})$$

and  $\mathbf{e}(t)$  a six-dimensional vector process depending on the components of strain tensor  $[\varepsilon(t)]$ , i.e.:

$$\mathbf{e}(t) = \begin{bmatrix} \varepsilon_x(t) & \varepsilon_y(t) & \varepsilon_z(t) & \frac{\gamma_{xy}(t)}{2} & \frac{\gamma_{xz}(t)}{2} & \frac{\gamma_{yz}(t)}{2} \end{bmatrix}. \quad (\text{A11})$$

Vector of direction cosines  $\mathbf{d}$  can also be expressed through angles  $\phi$ ,  $\theta$  and  $\alpha$ , as follows [27]:

$$\mathbf{d} = \begin{bmatrix} d_1 \\ d_2 \\ d_3 \\ d_4 \\ d_5 \\ d_6 \end{bmatrix} = \begin{bmatrix} \frac{1}{2} [\sin(\theta) \sin(2\phi) \cos(\alpha) + \sin(\alpha) \sin(2\theta) \cos(\phi)^2] \\ \frac{1}{2} [-\sin(\theta) \sin(2\phi) \cos(\alpha) + \sin(\alpha) \sin(2\theta) \sin(\phi)^2] \\ 1 \\ -\frac{1}{2} \sin(\alpha) \sin(2\theta) \\ \frac{1}{2} \sin(\alpha) \sin(2\phi) \sin(2\theta) - \cos(\alpha) \cos(2\phi) \sin(\theta) \\ \sin(\alpha) \cos(\phi) \cos(2\theta) + \cos(\alpha) \sin(\phi) \cos(\theta) \\ \sin(\alpha) \sin(\phi) \cos(2\theta) - \cos(\alpha) \cos(\phi) \cos(\theta) \end{bmatrix}. \quad (\text{A12})$$

Therefore, the variance of the shear strain resolved along generic direction  $q$  can be expressed in the following simplified form:

$$\text{Var}\left[\frac{\gamma_q(t)}{2}\right] = \text{Var}\left[\sum_k d_k e_k(t)\right] = \sum_i \sum_j d_i d_j \text{Cov}[e_i(t), e_j(t)] \quad (\text{A13})$$

By defining symmetric matrix [C] as:

$$[C] = \begin{bmatrix} V_x & C_{x,y} & C_{x,z} & C_{x,xy} & C_{x,xz} & C_{x,yz} \\ C_{x,y} & V_y & C_{y,z} & C_{y,xy} & C_{y,xz} & C_{y,yz} \\ C_{x,z} & C_{y,z} & V_z & C_{z,xy} & C_{z,xz} & C_{z,yz} \\ C_{x,xy} & C_{y,xy} & C_{z,xy} & V_x & C_{xy,xz} & C_{xy,yz} \\ C_{x,xz} & C_{y,xz} & C_{z,xz} & C_{xy,xz} & V_x & C_{xz,yz} \\ C_{x,yz} & C_{y,yz} & C_{z,yz} & C_{xy,yz} & C_{xy,yz} & V_y \end{bmatrix} \quad (\text{A14})$$

where (for  $i, j=x, y, z$ ):

$$V_i = \text{Var}[\varepsilon_i(t)] \quad (\text{A15})$$

$$V_i = \text{Var}\left[\frac{\gamma_{ij}(t)}{2}\right] \quad (\text{A16})$$

$$C_{i,j} = \text{CoVar}\left[\varepsilon_i(t), \varepsilon_j(t)\right] \quad (\text{A17})$$

$$C_{ij,i} = \text{CoVar}\left[\frac{\gamma_{ij}(t)}{2}, \varepsilon_i(t)\right] \quad (\text{A18})$$

$$C_{i,ij} = \text{CoVar}\left[\varepsilon_i(t), \frac{\gamma_{ij}(t)}{2}\right] \quad (\text{A19})$$

$$C_{ij,ij} = \text{CoVar}\left[\frac{\gamma_{ij}(t)}{2}, \frac{\gamma_{ij}(t)}{2}\right] \quad (\text{A20})$$

Eq. (A13) can easily be rewritten as follows:

$$\text{Var}\left[\frac{\gamma_q(t)}{2}\right] = \mathbf{d}^T [C] \mathbf{d}. \quad (\text{A21})$$

The global maxima of Eq. (A21) allow the directions experiencing the maximum variance of the resolved shear stress to be determined directly. In particular, the problem to be solved is nothing

but a conventional optimisation problem which can easily be addressed by using standard methodologies such as the gradient ascent technique [27].

Amongst all the selected planes containing a direction experiencing the maximum variance of the resolved shear strain, according to the fatigue damage model depicted in Figure 1a, the critical plane is then the one associated with the largest value of ratio  $\rho$ , Eq. (1). Finally, if  $\theta^*$ ,  $\phi^*$  and  $\alpha^*$  are used to denote the angles defining the orientation of this plane together with the associated critical direction MV, the stress and strain components relative to the critical plane can directly be determined via Eqs (A5) to (A8), where  $\theta=\theta^*$ ,  $\phi=\phi^*$  and  $\alpha=\alpha^*$ .

### Acknowledgements

The Jiangsu Oversea Research & Training Program for University Prominent Young & Middle-aged Teachers and the National Natural Science Foundation of China are acknowledged for supporting the present research project (Project No.: 10702027).

### References

- [1] Langlais TE, Vogel JH, Chase TR. Multiaxial cycle counting for critical plane methods. *Int J Fatigue* 2003;25:641-647.
- [2] Wang CH, Brown MW. Life prediction techniques for variable amplitude multiaxial fatigue – Part 1: Theories. *Trans. ASME, J. Eng. Mat. Techn.* 1996;118:367-370.
- [3] Wang CH, Brown MW. Life prediction techniques for variable amplitude multiaxial fatigue – Part 2: Comparison with experimental results. *Trans. ASME, J. Eng. Mat. Techn.* 1996;118:371-374.
- [4] Kim KS, Park JC, Lee JW. Multiaxial fatigue under variable amplitude loads. *Trans. ASME, J. Eng. Mat. Techn.* 1999;121:286-293.
- [5] Kim KS, Park JC. Shear strain based multiaxial fatigue parameters applied to variable amplitude loading. *Int J Fatigue* 1999;21:475-483.
- [6] Chen X, Jin D, Kim S. A weight function-critical plane approach for low-cycle fatigue under variable amplitude multiaxial loading. *Fatigue Fract Engng Mater Struct* 2006;29:331-339.
- [7] Socie DF, Marquis GB. *Multiaxial Fatigue*, SAE, Warrendale, PA, 2000.
- [8] Smith KN, Watson P, Topper TH. A stress-strain function for the fatigue of metals. *J Mater.* 1970;5:767-776.
- [9] Socie DF. Fatigue damage models. *Trans. ASME, J. Eng. Mat. Techn.* 1987;109:293-298.
- [10] Kandil FA, Brown MW, Miller KJ. Biaxial low-cycle fatigue fracture of 316 stainless steel at elevated temperature. *Met. Soc. London* 1982;280:203-210.
- [11] Wang CH, Brown MW. A path-independent parameter for fatigue under proportional and non-proportional loading. *Fatigue Fract Engng Mater Struct* 1993;16:1285-1298.
- [12] Fatemi A, Socie DF. A critical plane approach to multiaxial fatigue damage including out-of-phase loading. *Fatigue Fract Engng Mater Struct* 1988;11:149-165.
- [13] Bannantine JA, Socie DF. A variable amplitude multiaxial life prediction method. In: *Fatigue under Biaxial and Multiaxial Loading*, Edited by K. Kussmaul, D. McDiarmid and D. Socie, ESIS 10, Mechanical Engineering Publications, London, pp. 35-51, 1991.

- [14] Shamsaei N, Gladskyi M, Panasovskyi K, Shukaev S, Fatemi A. Multiaxial fatigue of titanium including step loading and load path alteration and sequence effects. *Int J Fatigue* 2010;32:1862-1874.
- [15] Shamsaei N, Fatemi A, Socie DF. Multiaxial fatigue evaluation using discriminating strain paths. *Int J Fatigue* 2011;33:597-609.
- [16] Matsuishi M, Endo T. Fatigue of metals subjected to varying stress. Presented to the Japan Society of Mechanical Engineers, Fukuoka, Japan; 1968.
- [17] Fatemi A, Yang L. Cumulative fatigue damage and life prediction theories: a survey of the state of the art for homogeneous materials. *Int J Fatigue* 1998;20(1):9-34.
- [18] Palmgren A. Die Lebensdauer von Kugellagern. vol. 68. *Verfahrenstechnik*, Berlin, 1924. p. 339-41.
- [19] Miner MA. Cumulative damage in fatigue. *J Appl Mech* 1945;67:AI59-64.
- [20] Sonsino CM. Fatigue testing under variable amplitude loading. *Int J Fatigue* 2007;29 6:1080-9.
- [21] Sonsino CM, Kueppers M. Multiaxial fatigue of welded joints under constant and variable amplitude loadings. *Fatigue Fract Eng Mater Struct* 2001;24:309-27.
- [22] Chen X, Jin D, Kim KS. Fatigue life prediction of type 304 stainless steel under sequential biaxial loading. *Int J Fatigue* 2006;28:289-299.
- [23] Susmel L, Meneghetti G, Atzori B. A simple and efficient reformulation of the classical Manson-Coffin curve to predict lifetime under multiaxial fatigue loading. Part I: plain materials. *Trans ASME, J Eng Mat Techn* 2009;131(2):021009-1/9.
- [24] Susmel L, Meneghetti G, Atzori B. A simple and efficient reformulation of the classical Manson-Coffin curve to predict lifetime under multiaxial fatigue loading. Part II: notches. *Trans ASME, J Eng Mat Techn* 2009;131(2):021010-1/8.
- [25] Susmel L, Atzori B, Meneghetti G, Taylor D. Notch and Mean Stress Effect in Fatigue as Phenomena of Elasto-Plastic Inherent Multiaxiality. *Engineering Fracture Mechanics* 2011;78:1628-1643.
- [26] Macha E. Simulation investigations of the position of fatigue fracture plane in materials with biaxial loads. *Materialwiss Werkstofftech* 1989;20(4):132-6.
- [27] Susmel L. A simple and efficient numerical algorithm to determine the orientation of the critical plane in multiaxial fatigue problems. *Int J Fatigue* 2010;32:1875-1883.
- [28] Susmel L, Tovo R, Socie DF. Estimating the orientation of Stage I crack paths through the direction of maximum variance of the resolved shear stress. *Int J Fatigue* 2014;58:94-101.
- [29] Kanazawa K, Miller KJ, Brown MW. Low-cycle fatigue under out-of phase loading conditions. *Trans ASME, J Eng Mat Techn* 1977:222-228.
- [30] Socie D, Bannantine J. Bulk Deformation Damage Models. *Materials Science and Engineering* 1988;A103:3-13.
- [31] Susmel L. *Multiaxial Notch Fatigue: from nominal to local stress-strain quantities*. Woodhead & CRC, Cambridge, UK, 2009.
- [32] Kaufman RP, Topper T. The influence of static mean stresses applied normal to the maximum shear planes in multiaxial fatigue. In: *Biaxial and Multiaxial fatigue and Fracture*, Edited by A. Carpinteri, M. de Freitas and A. Spagnoli, Elsevier and ESIS, 2003, pp. 123-143.
- [33] Benasciutti D, Tovo R. Spectral methods for lifetime prediction under wide-band stationary random processes. *Int J Fatigue* 2005;27:867-877.

- [34] Benasciutti D, Tovo R. Cycle distribution and fatigue damage assessment in broad-band non-Gaussian random processes. *Probab Eng Mech* 2005;20:115-127.
- [35] Susmel L, Tovo R, Benasciutti D. A novel engineering method based on the critical plane concept to estimate lifetime of weldments subjected to variable amplitude multiaxial fatigue loading. *Fatigue Fract Engng Mater Struct* 2009;32:441-459.
- [36] Susmel L. Estimating fatigue lifetime of steel weldments locally damaged by variable amplitude multiaxial stress fields. *Int J Fatigue* 2010;32:1057-1080.
- [37] Susmel L, Tovo R. Estimating Fatigue Damage under Variable Amplitude Multiaxial Fatigue Loading. *Fatigue Fract Engng Mater Struct* 2011;34:1053-1077.
- [38] Susmel L, Taylor D. A critical distance/plane method to estimate finite life of notched components under variable amplitude uniaxial/multiaxial fatigue loading. *Int J Fatigue* 2012;38:7-24.
- [39] Louks R, Gerin B, Draper J, Askes H, Susmel L. On the multiaxial fatigue assessment of complex three-dimensional stress concentrators. *Int J Fatigue* 2014;63:12-24.
- [40] Susmel L. Four stress analysis strategies to use the Modified Wöhler Curve Method to perform the fatigue assessment of weldments subjected to constant and variable amplitude multiaxial fatigue loading. *Int J Fatigue* 2014;64:38-54.
- [41] Zhao T, Jiang Y. Fatigue of 7075-T651 aluminium alloy. *Int J Fatigue* 2008;30:834-849.
- [42] Hoffmeyer J, Döring R, Seeger T, Vormwald M. Deformation behaviour, short crack growth and fatigue lives under multiaxial nonproportional loading. *Int J Fatigue* 2006;28:508-520.
- [43] Lin H, Nayeb-Hashemi H, Pelloux RM. Constitutive relations and fatigue life prediction for anisotropic al-6061-t6 rods under biaxial proportional loadings. *Int J Fatigue* 1992;14:249-259.
- [44] Shang DG, Sun GQ, Yan CL. Multiaxial fatigue damage parameter and life prediction for medium-carbon steel based on the critical plane approach. *Int J Fatigue* 2007;29:2200-2207.
- [45] Hua CT, Socie DF. Fatigue damage in 1045 steel under constant amplitude biaxial loading. *Fatigue Fract Eng Mater Struct* 1984;7:165-179.
- [46] Kurath P, Downing SD, Galliard DR. Summary of non-hardened notched shaft-round robin program. multiaxial fatigue-analysis and experiments. G. E. Leese and D. F. Socie, eds., SAE, Warrendale, PA, 1989:AE-14:13-32.
- [47] Nelson DV, Rostami A. Biaxial fatigue of A533B pressure vessel steel. *ASME J. Pressure Vessel Technol.* 1997;119:325-331.
- [48] Jiang Y, Hertel O, Vormwald M. An experimental evaluation of three critical plane multiaxial fatigue criteria. *Int J Fatigue* 2007;29:1490-1502.
- [49] Hertel O, Vormwald M. Short-crack-growth-based fatigue assessment of notched components under multiaxial variable amplitude loading. *Eng Frac Mech* 2011;78: 1614-1627.
- [50] Chen X, An K, Kim KS. Low-Cycle Fatigue of 1Cr-18Ni-9Ti Stainless Steel and Related Weld Metal Under Axial, Torsional and 90° Out-of-Phase-Loading. *Fatigue Fract Eng Mater Struct* 2004;27:439-448.
- [51] Socie DF, Waill LA, Dittmer DF. Biaxial Fatigue of Inconel 718 Including Mean Stress Effects. In: *Multiaxial Fatigue*, ASTM STP 853, K. J. Miller and M. W. Brown, eds., American Society for Testing and Materials, Philadelphia, PA, 1985:463-481.
- [52] Socie DF, Kurath P, Koch J. A multiaxial fatigue damage parameter. *Biaxial and Multiaxial Fatigue*, EGF 3, M. W. Brown and K. J. Miller, eds., Mechanical Engineering, London, 1989:535-550.

- [53] Kim KS, Lee BL, Park JC. Biaxial Fatigue of Stainless Steel 304 under irregular loading. *Fatigue and Fracture Mechanics: 31<sup>st</sup> Volume*, ASTM STP 1389, G. R. Halford and J. P. Gallagher, Eds., ASTM, West Conshohocken, PA, 2000:79-93.
- [54] Chen X, Jin D, Kim KS. Fatigue life prediction of type 304 stainless steel under sequential biaxial loading. *Int J Fatigue* 2006;28:289-299.
- [55] Lee BL, Kim KS, Nam KM. Fatigue analysis under variable amplitude loading using an energy parameter. *Int J Fatigue* 2003;25:621-631.
- [56] Han C, Chen X, Kim KS. Evaluation of multiaxial fatigue criteria under irregular loading. *Int J Fatigue* 2002;24:913-922.
- [57] Shamsaei N, Fatemi A. Effect of hardness on multiaxial fatigue behaviour and some simple approximations for steels. *Fatigue Fract Engng Mater Struct* 2009;32:631-646.
- [58] Lee Y-L, Pan J, Hathaway RB, Barkey ME. *Fatigue Testing and Analysis*. Elsevier Butterworth-Heinemann, Oxford, UK, 2005 (ISBN: ISBN 0-7506-7719-8).
- [59] Jiang, Y., and Sehitoglu, H., 1996, "Modelling of Cyclic Ratchetting Plasticity—Part I: Development and Constitutive Relations," *ASME Trans. J. Appl. Mech.*, 63, pp. 720-725.
- [60] Jiang, Y., and Sehitoglu, H., 1996, "Modelling of Cyclic Ratchetting Plasticity—Part II: Comparison of Model Simulations With Experiments," *ASME Trans. J. Appl. Mech.*, 63, pp. 726-733.

## List of Captions

- Table 1:** Static and fatigue properties of the investigated materials Static and fatigue properties of the investigated materials (values in bold indicate the material constants being estimated; values in italic indicate the material constant being determined by post-processing the provided experimental results generated under fully-reversed axial loading and fully-reversed torsion).
- Figure 1:** Fatigue damage model (a) and modified Manson-Coffin diagram (b).
- Figure 2:** Adopted definitions to calculate the amplitude and the mean value of the stress components relative to the critical plane under both constant and variable amplitude fatigue loading.
- Figure 3:** In-field use of the MMCCM applied along with the  $\gamma$ -MVM to estimate fatigue lifetime under constant amplitude fatigue loading.
- Figure 4:** In-field use of the MMCCM applied along with the  $\gamma$ -MVM to estimate fatigue lifetime under variable amplitude fatigue loading.
- Figure 5:** Reference loading paths (IPh=in-phase; OoPh=out-of-phase, ZMS=zero mean strain; N-ZMS=non-zero mean strain).
- Figure 6:** Determination of the reference error band (a); accuracy of the MMCCM in predicting fatigue lifetime under CA nominal loading paths (b) – see also Figure 5.
- Figure 7:** Specimens of S460N [48], Al 7075-T651 [41] and 304SS [54] tested under combined axial and torsional CA strain signals of different frequencies.
- Figure 8:** Specimens of 304SS [48], pure titanium [14], titanium BT9 [14], SNCM439 [55], SNCM630 (A) [56] and SNCM630 (B) [55] tested under fully-reversed sequential loading (A=Axial cyclic loading; T=torsional cyclic loading; I=in-phase axial loading and torsion; O=90° out-of-phase axial loading and torsion).
- Figure 9:** Specimens of S45C [4], 304SS [53], SNCM439 [55], SNCM630 (A) [56] and SNCM630 (B) [55] subjected to short variable amplitude load histories.
- Figure 10:** Specimens of 1045 QT [15] and 304L [15] subjected to discriminating strain paths.
- Figure 11:** Specimens of Al5083 [49] and S460N [49] subjected to short variable amplitude load histories.
- Figure A1:** Definition of angles  $\alpha$ ,  $\phi$ , and  $\theta$ .

## Tables

Material	Ref.	E [GPa]	G [GPa]	K' [MPa]	n'	$\sigma'_f$ [MPa]	$\epsilon'_f$	b	c	$\tau'_f$ [MPa]	$\gamma'_f$	b <sub>0</sub>	c <sub>0</sub>
Al7075-T651	[41]	71.7	27.5	790	0.064	1104	0.519	-0.118	-0.87	687	1.346	-0.112	-0.993
Al5083	[42]	68	25.6	544	0.075	780	1.153	-0.114	-0.861	<b>451</b>	<b>1.997</b>	<b>-0.114</b>	<b>-0.861</b>
6061-T6 (A)	[43]	71.5	28.2	436	0.069	369	0.09	-0.031	-0.45	285	0.3881	-0.05	-0.642
6061-T6 (B)	[43]	71.5	28.2	436	0.069	373	0.104	-0.033	-0.473	245	1.4746	-0.048	-0.675
S45C	[4]	186	70.6	1215	0.217	923	0.359	-0.099	-0.519	685	0.198	-0.12	-0.36
45 Steel	[44]	190	7	1258	0.208	843	0.327	-0.105	-0.546	559	0.496	-0.108	-0.469
SAE 1045	[45, 46]	204	80.3	1258	0.208	930	0.298	-0.106	-0.49	505	0.413	-0.097	-0.445
A533B	[47]	193	76.1	827	0.13	847	1.201	-0.083	-0.64	586	1.554	-0.115	-0.615
S460N	[48, 49]	208.5	80.2	1115	0.161	834	0.1572	-0.079	-0.493	529	0.213	-0.096	-0.418
AISI 304	[9]	183	82.8	1660	0.287	1000	0.171	-0.114	-0.402	640	0.279	-0.124	-0.339
1Cr-18Ni-9Ti	[50]	193	74.3	1115	0.1304	1104	0.8072	-0.091	-0.665	644	0.8118	-0.088	-0.533
Inconel 718	[51, 52]	208.5	77.8	1530	0.07	1640	2.67	-0.06	-0.82	1030	3.62	-0.074	-0.778
304SS	[53-55]	171	66	812	0.125	760	0.0763	-0.079	-0.36	627	0.193	-0.078	-0.369
SNCM630 (A)	[56]	196	77	1056	0.054	1272	1.54	-0.073	-0.823	858	1.51	-0.061	-0.706
1050 QT	[15, 57]	203	81	-	-	1346	2.01	-0.062	-0.725	<b>777</b>	<b>3.481</b>	<b>-0.062</b>	<b>-0.725</b>
SNCM439	[55]	208	80.2	1234	0.102	1050	1.426	-0.054	-0.786	<b>606</b>	<b>2.47</b>	<b>-0.054</b>	<b>-0.786</b>
SNCM630 (B)	[55]	196	77	926	0.032	1008	1.168	-0.042	-0.792	<b>582</b>	<b>2.023</b>	<b>-0.042</b>	<b>-0.792</b>
304L Stainless Steel	[15]	195	77	-	-	1287	0.122	-0.145	-0.394	<b>743</b>	<b>0.2113</b>	<b>-0.145</b>	<b>-0.394</b>
Pure Titanium	[14]	112	40	-	-	647	0.548	-0.033	-0.646	485	0.417	-0.069	-0.523
Titanium BT9	[14]	118	43	-	-	1180	0.278	-0.025	-0.665	881	0.18	-0.082	-0.47

**Table 1:** Static and fatigue properties of the investigated materials Static and fatigue properties of the investigated materials (values in bold indicate the material constants being estimated; values in italic indicate the material constant being determined by post-processing the provided experimental results generated under fully-reversed axial loading and fully-reversed torsion).

# Figures

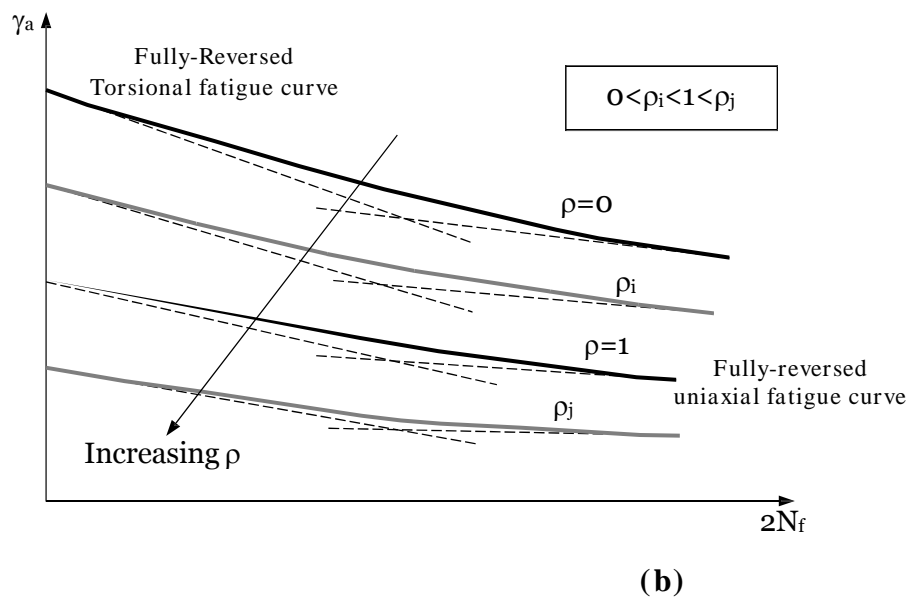
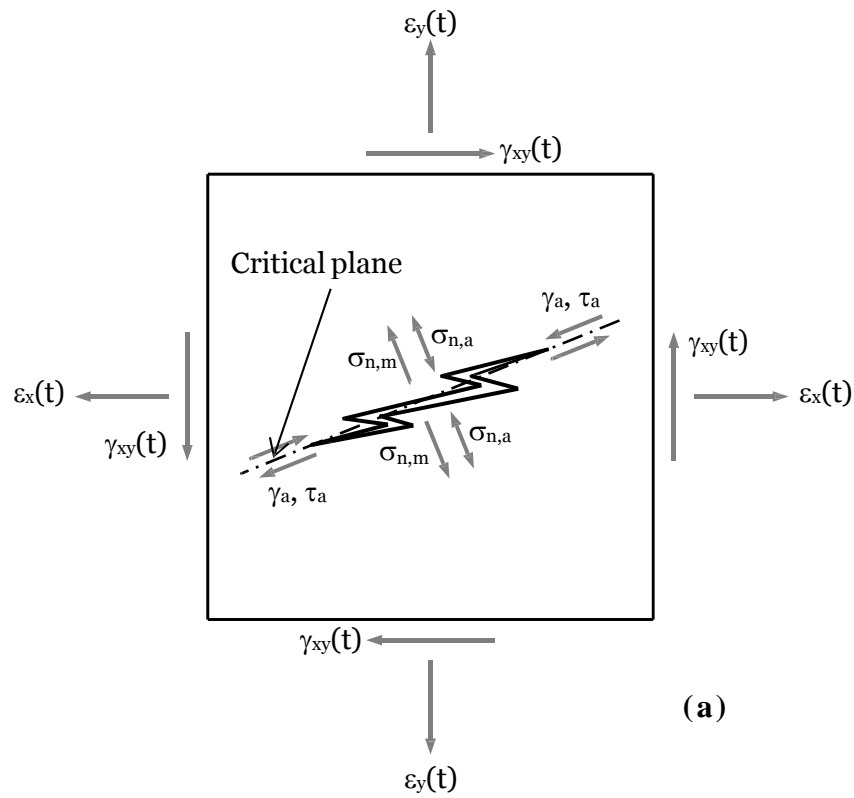
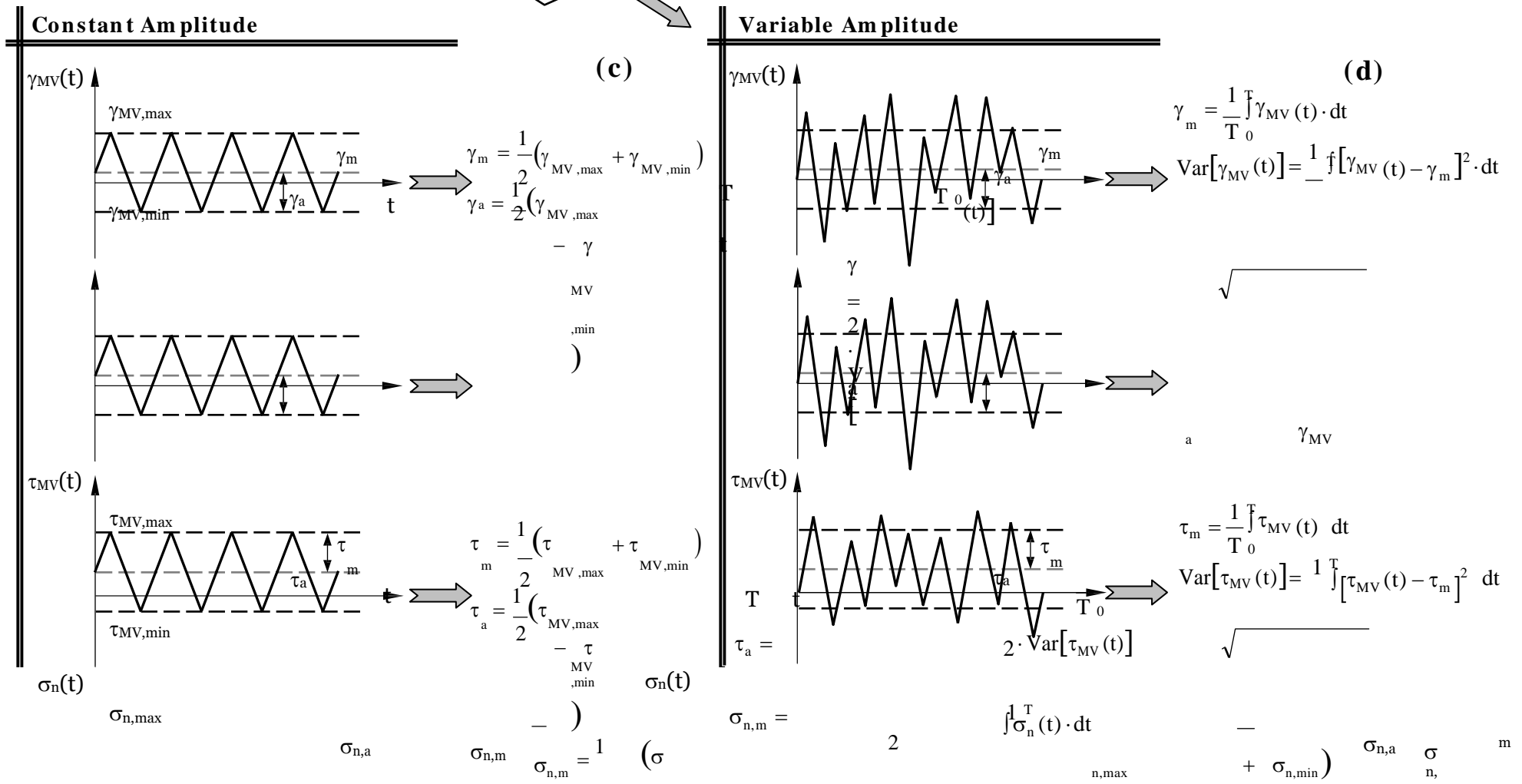
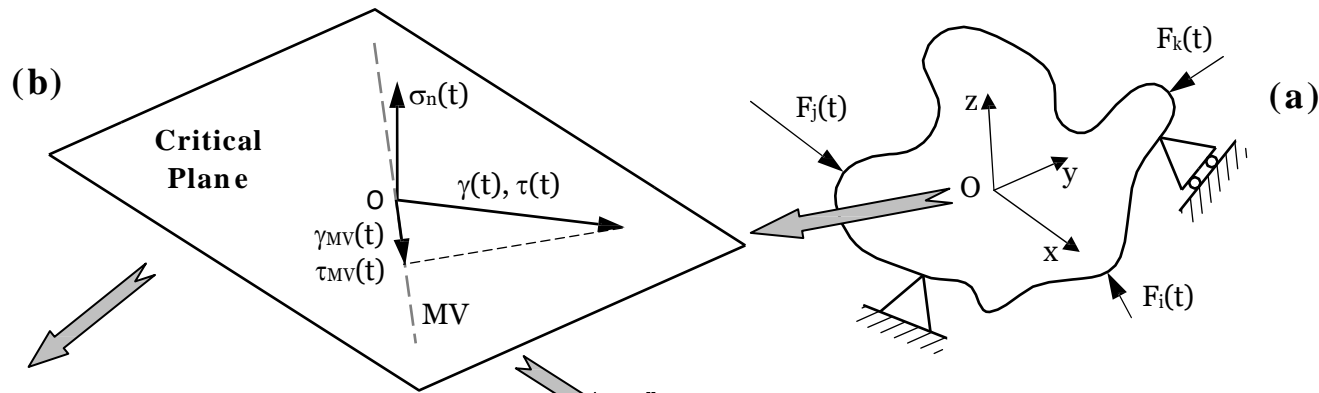


**Figure 1:** Fatigue damage model (a) and modified Manson-Coffin diagram (b).



$$\text{Var}[\sigma_n] = \frac{1}{T_0} \int_0^{T_0} [\sigma_n(t) - \sigma_{n,m}]^2 dt$$

$$\sigma_{n,a} = \frac{1}{2} (\sigma_{n,max} - \sigma_{n,min})$$

$$2 \cdot \text{Var}[\sigma_n] = \frac{1}{T_0} \int_0^{T_0} (\sigma_n(t) - \sigma_{n,m})^2 dt$$

**Figure 2:** Adopted definitions to calculate the amplitude and the mean value of the stress components relative to the critical plane under both constant and variable amplitude fatigue loading.

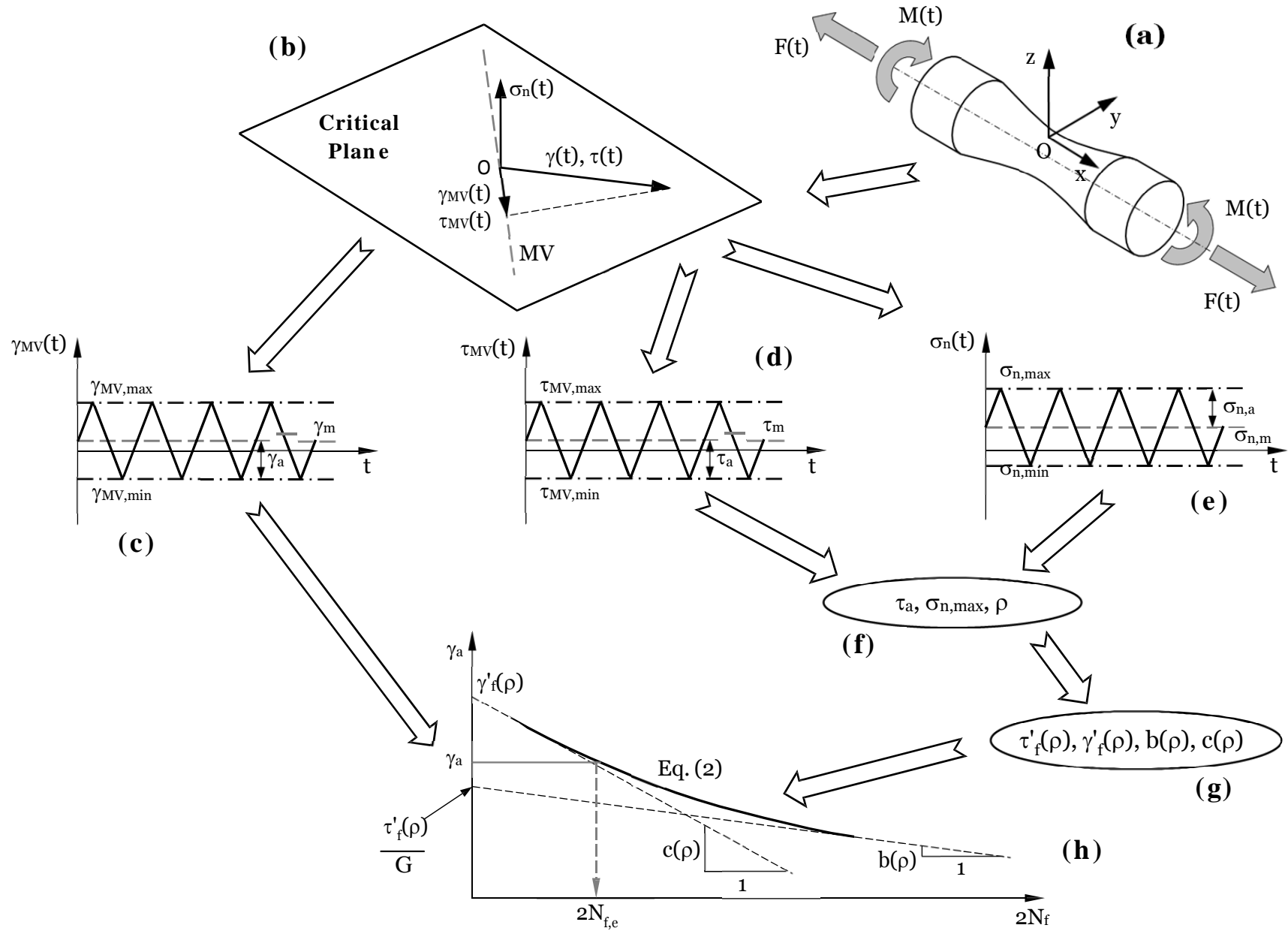


**Figure 3:** In-field use of the MMCCM applied along with the  $\gamma$ -MVM to estimate fatigue lifetime under constant amplitude fatigue loading.

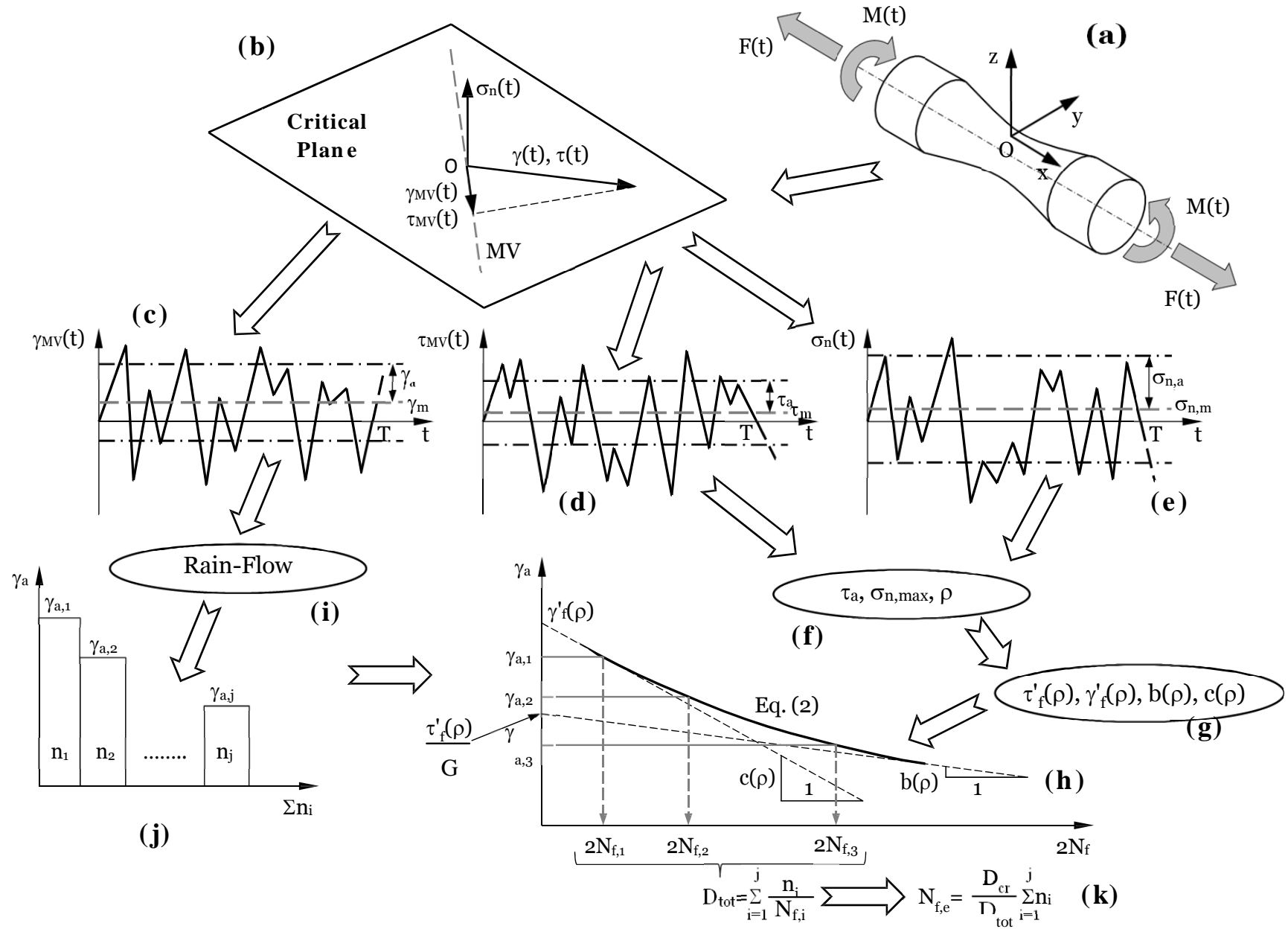


**Figure 4:** In-field use of the MMCCM applied along with the  $\gamma$ -MVM to estimate fatigue lifetime under variable amplitude fatigue loading.

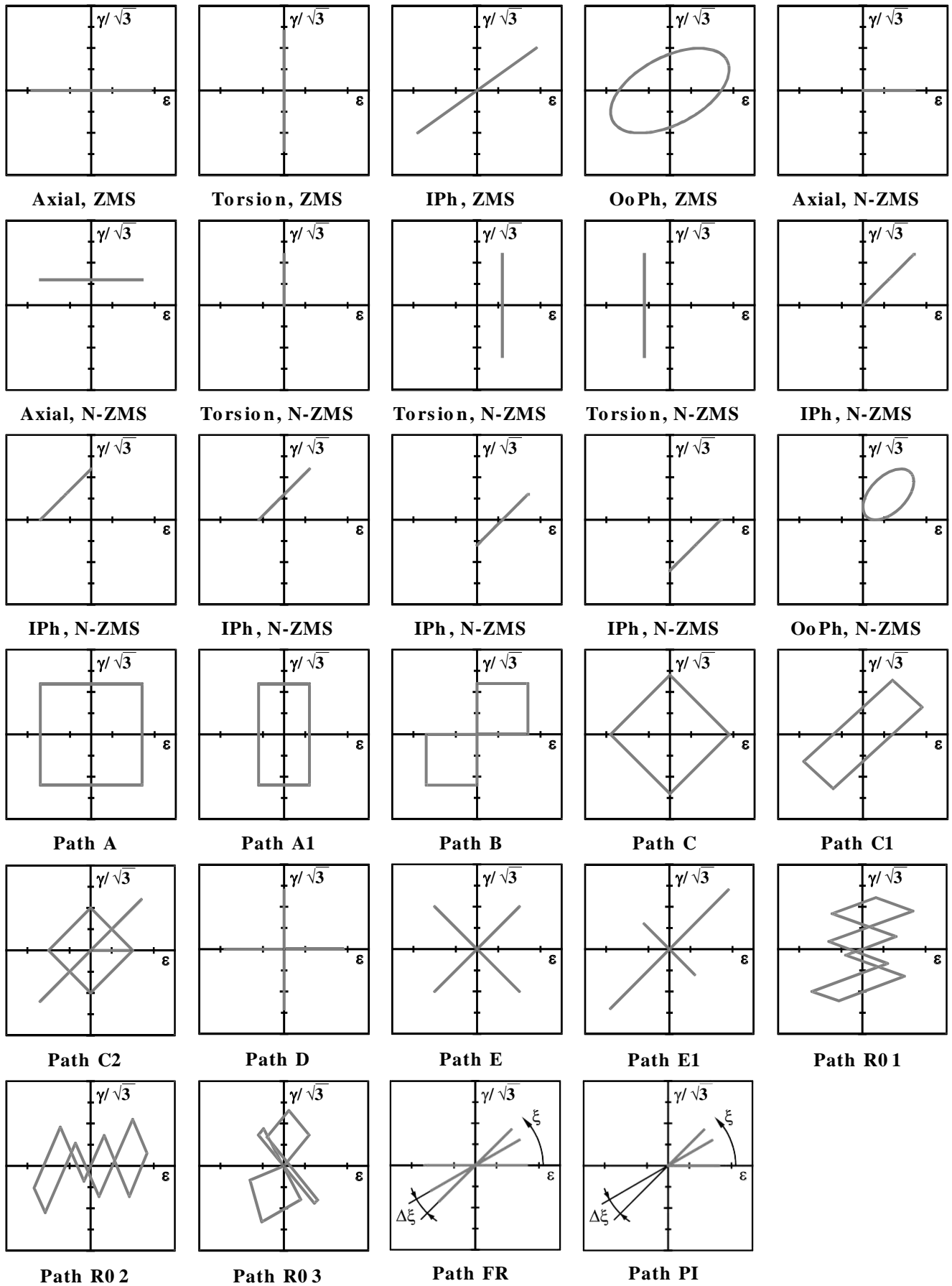


**Figure 5:** Reference loading paths (IPh=in-phase; OoPh=out-of-phase, ZMS=zero mean strain; N-ZMS=non-zero mean strain).

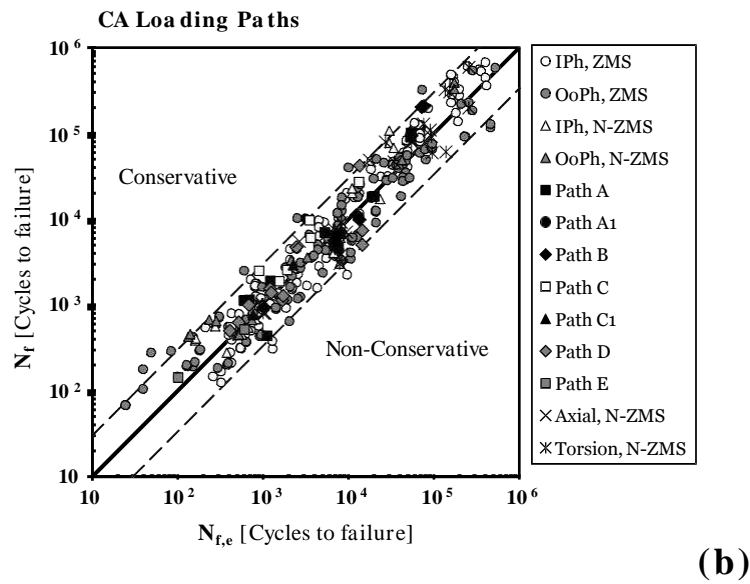
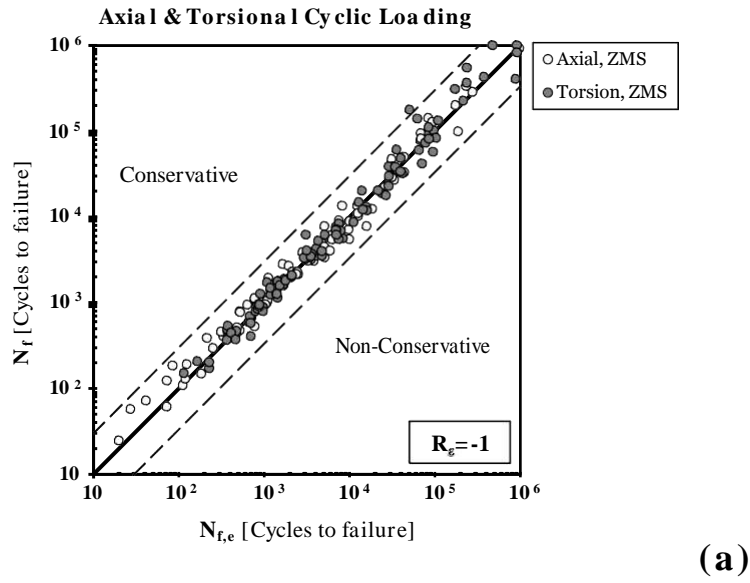


**Figure 6:** Determination of the reference error band (a); accuracy of the MMCCM in predicting fatigue lifetime under CA nominal loading paths (b) – see also Figure 5.

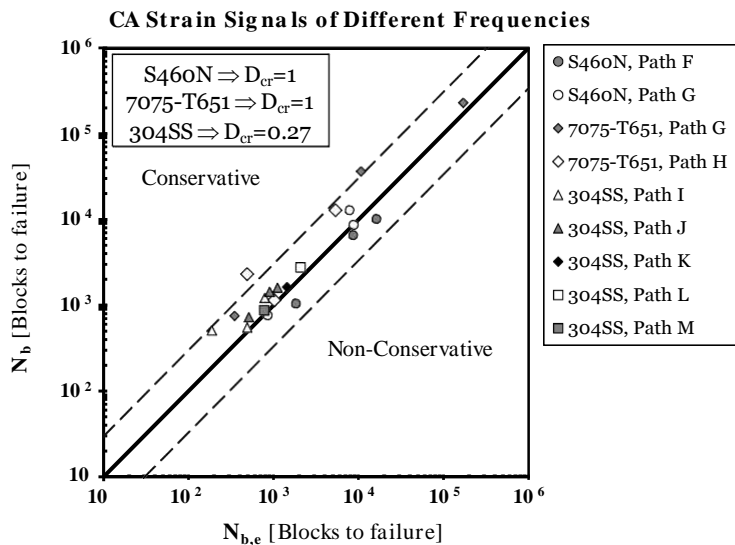
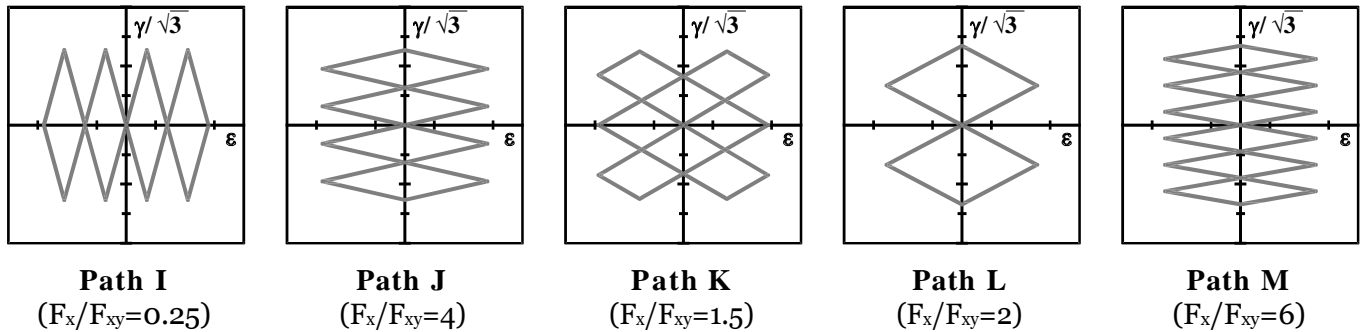
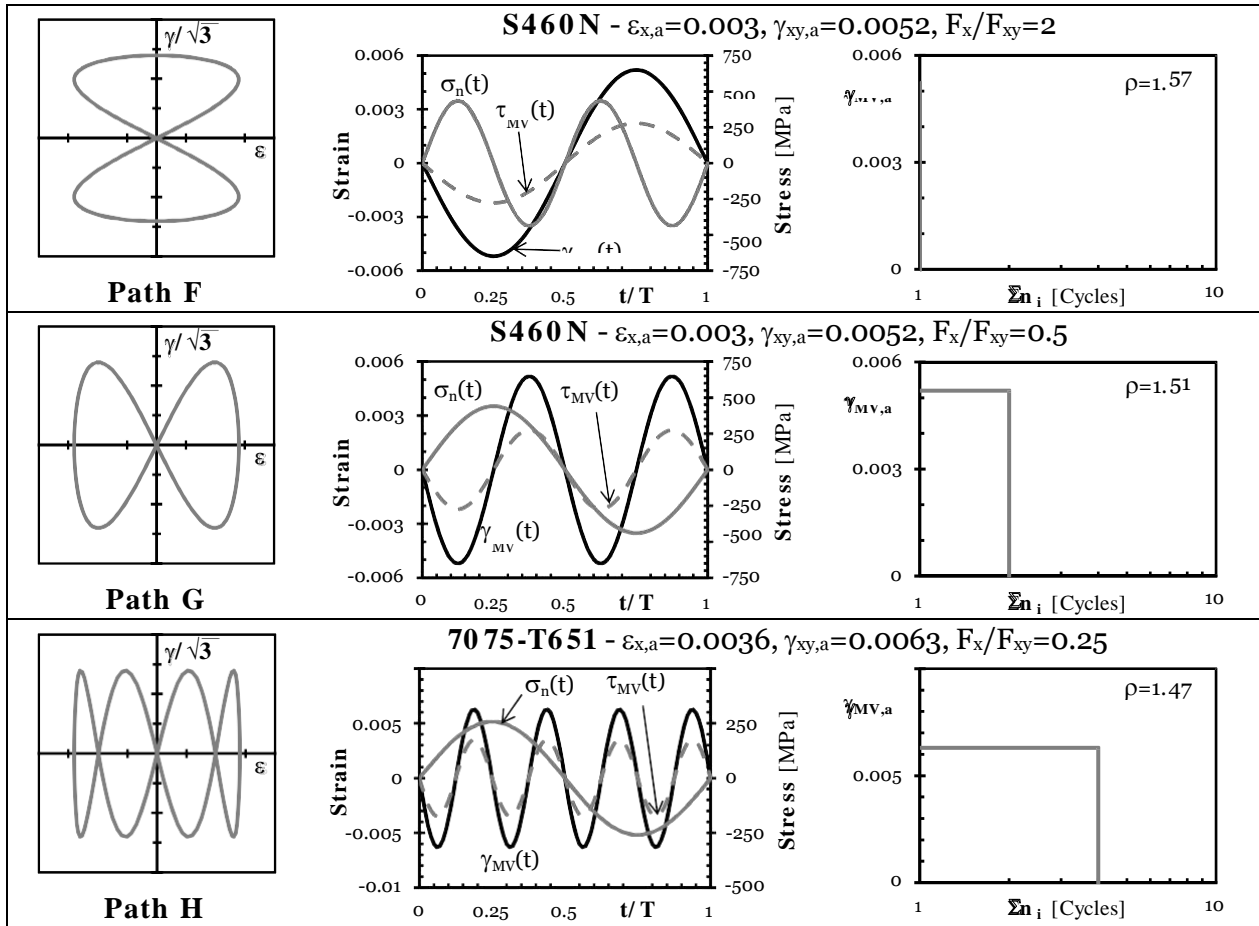


**Figure 7:** Specimens of S460N [48], Al 7075-T651 [41] and 304SS [54] tested under combined axial and torsional CA strain signals of different frequencies.

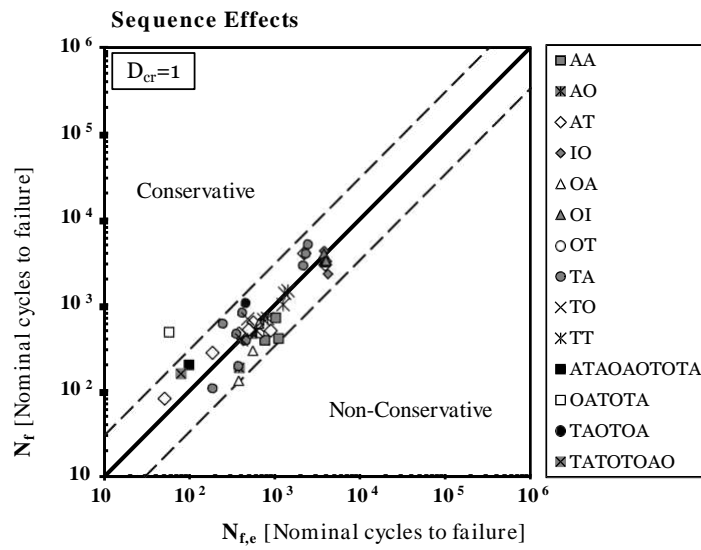


**Figure 8:** Specimens of 304SS [48], pure titanium [14], titanium BT9 [14], SNCM439 [55], SNCM630 (A) [56] and SNCM630 (B) [55] tested under fully-reversed sequential loading (A=Axial cyclic loading; T=torsional cyclic loading; I=in-phase axial loading and torsion; O=90° out-of-phase axial loading and torsion).

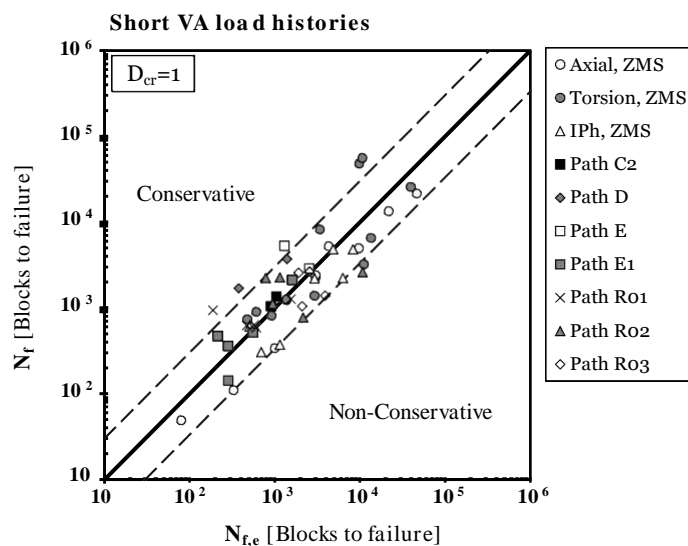
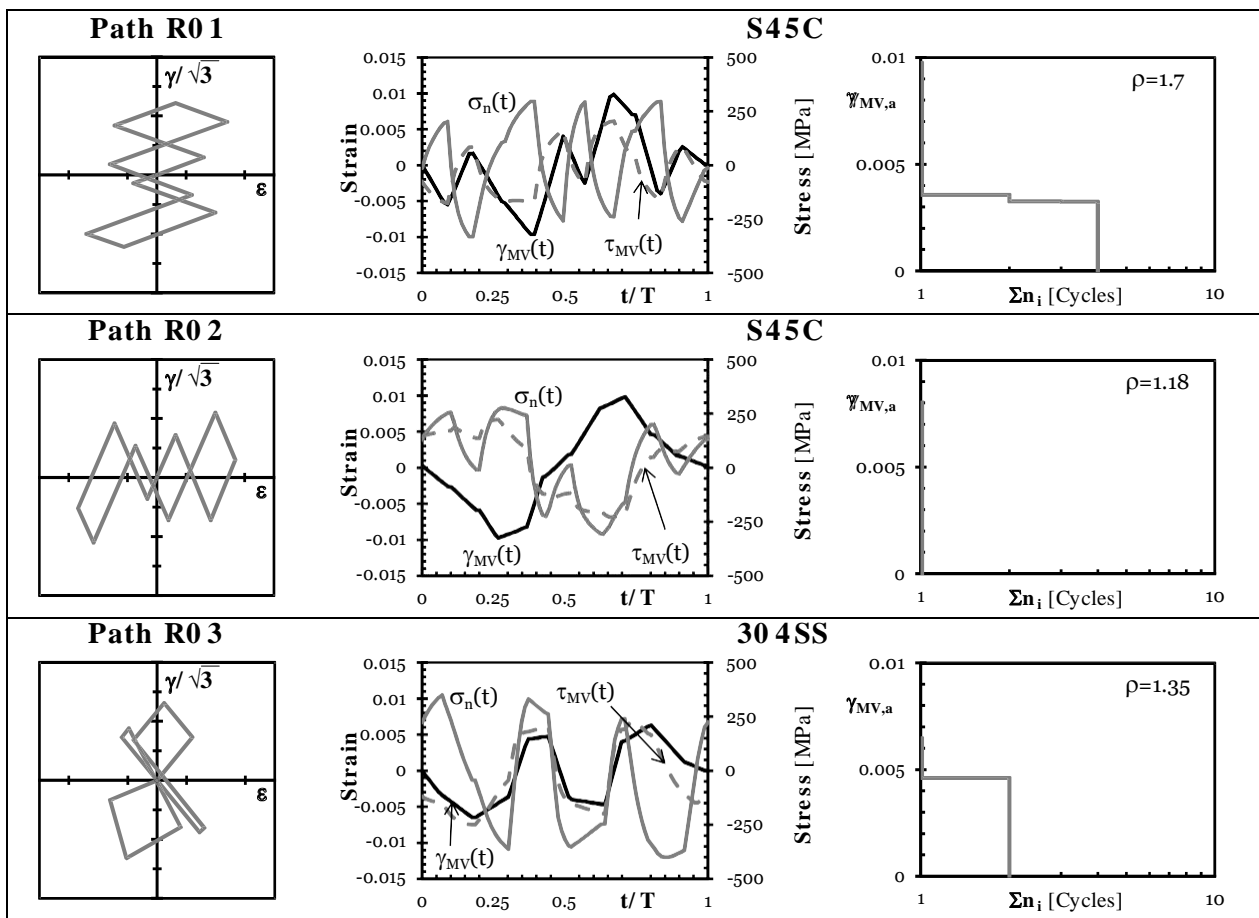


**Figure 9:** Specimens of S45C [4], 304SS [53], SNCM439 [55], SNCM630 (A) [56] and SNCM630 (B) [55] subjected to short variable amplitude load histories.

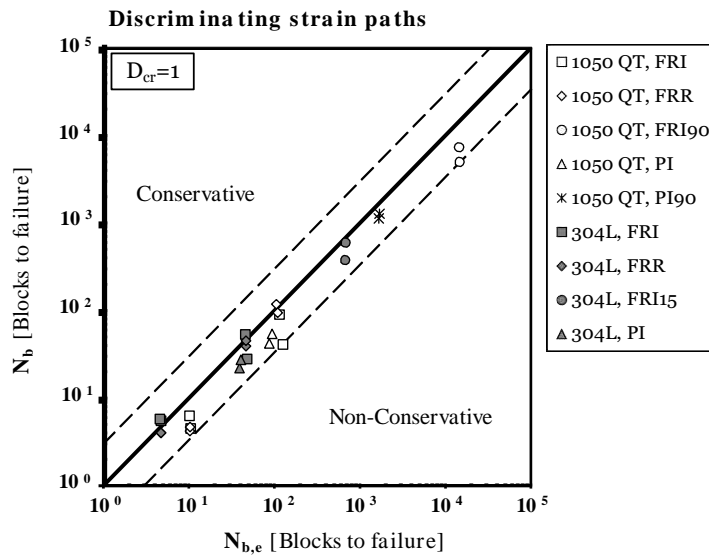
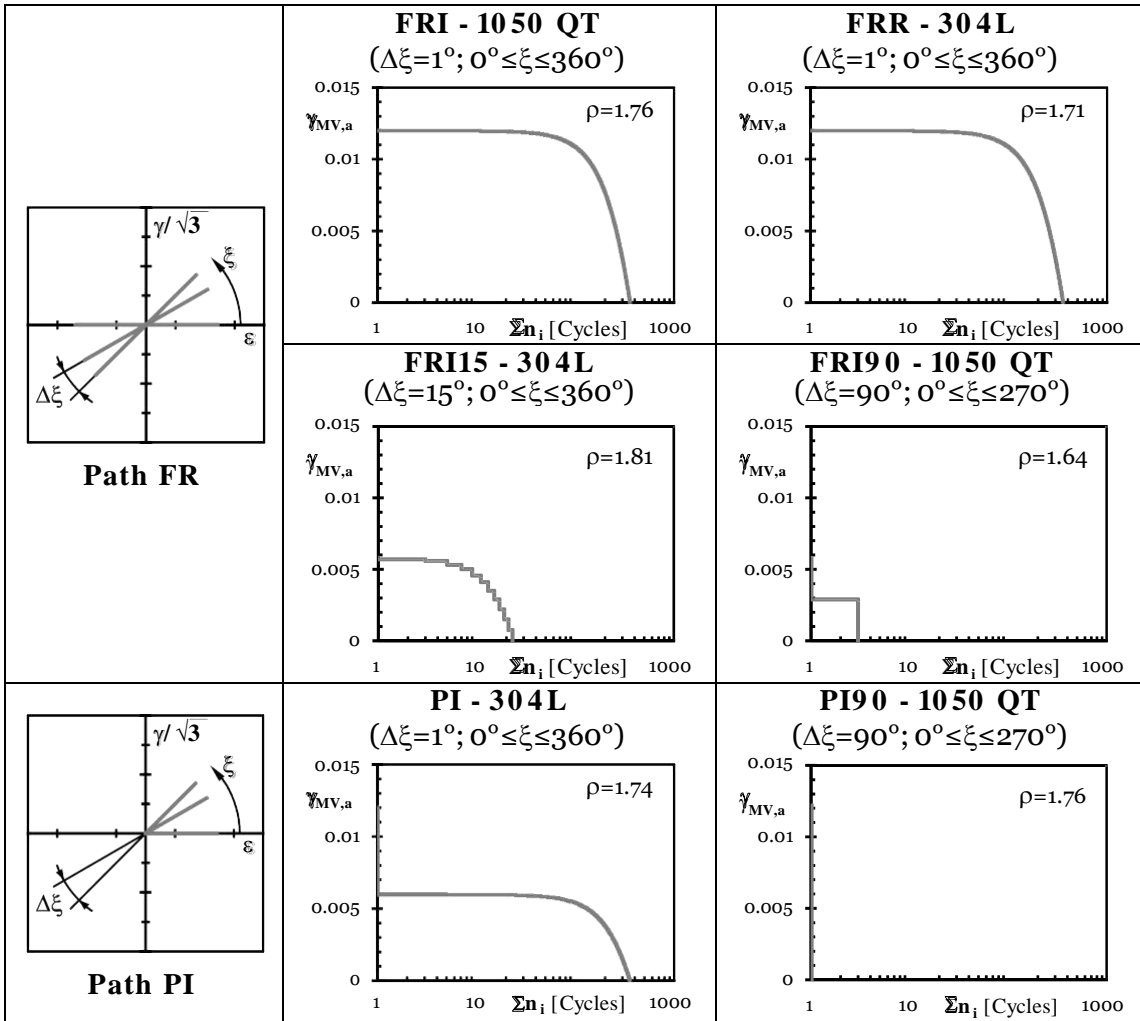


**Figure 10:** Specimens of 1045 QT [15] and 304L [15] subjected to discriminating strain paths.

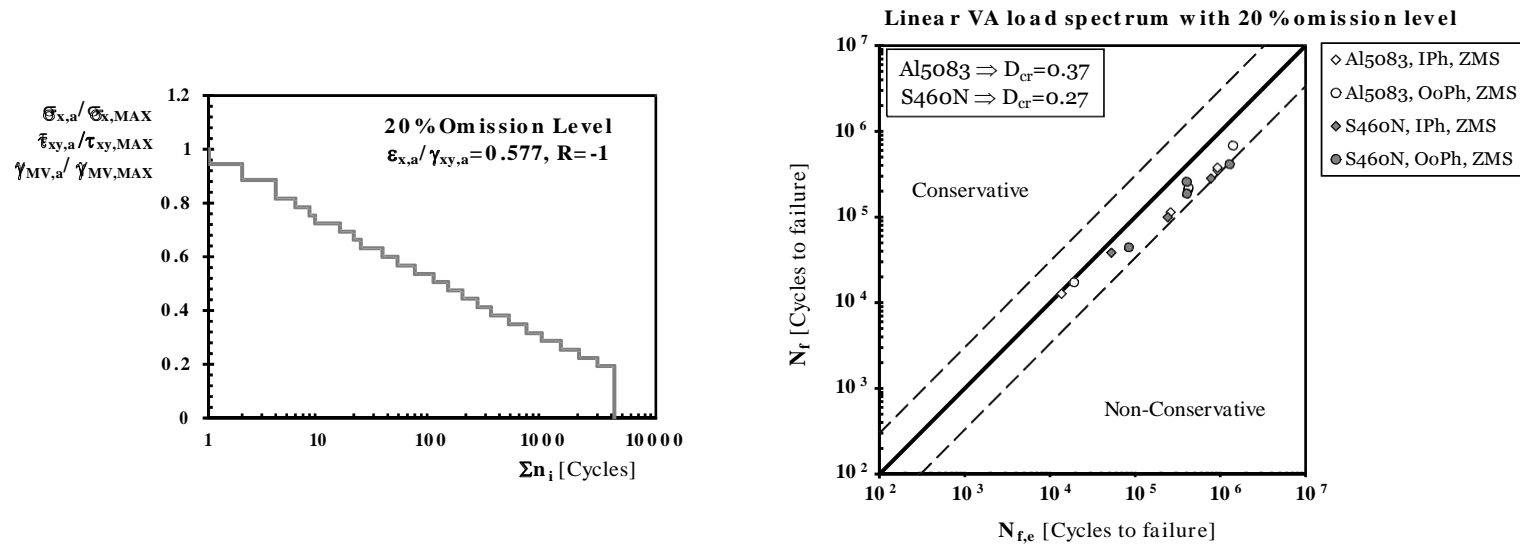


**Figure 11:** Specimens of Al5083 [49] and S460N [49] subjected to short variable amplitude load histories.

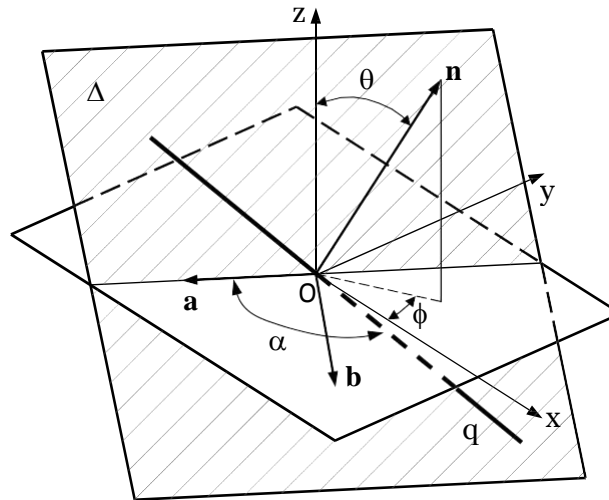


**Figure A1:** Definition of angles  $\alpha$ ,  $\phi$ , and  $\theta$ .